NOVA SCHOOL OF SCIENCE & TECHNOLOGY

DEPARTMENT OF MECHANICAL AND INDUSTRIAL ENGINEERING

MARCELO ANDRÉ ALKAIM DE MENEZES

BSc in Mechanical Engineering Sciences

DEVELOPMENT AND IMPROVEMENT OF A NUMERICAL MODEL TO SIMULATE THE MECHANICAL BEHAVIOUR OF RAILWAYS

MASTER IN MECHANICAL ENGINEERING

NOVA University Lisbon
March, 2023

DEPARTMENT OF MECHANICAL AND
INDUSTRIAL ENGINEERING

DEVELOPMENT AND IMPROVEMENT OF A NUMERICAL MODEL TO SIMULATE THE MECHANICAL BEHAVIOUR OF RAILWAYS

MARCELO ANDRÉ ALKAIM DE MENEZES

BSc in Mechanical Engineering Sciences

Adviser: Tiago Alexandre Narciso da Silva
Assistant Professor, NOVA University Lisbon

Co-adviser: Zuzana Dimitrovová
Assistant Professor, NOVA University Lisbon

MASTER IN MECHANICAL ENGINEERING

NOVA University Lisbon
March, 2023

Development and improvement of a numerical model to simulate the mechanical behaviour of railways

This document was created with the (pdf/Xe/Lua)LaTeX processor and the NOVAthesis template (v6.9.10) [1].

To you.

Acknowledgements

To my family, everyone who helped shape the person that I am, from my qualities to my faults. We all did - and still do - the best we could, and I am very grateful for that.

To my friends, not only for the sleepless nights, but also for the ones where they helped me sleep.

To my advisors, who were more than mere teachers, and to NOVA-SST, the institution which gave me awareness of thought, where I learned, not only about the absolute relativity of truth, but also that, in order to keep learning, one has to be aware of how little knowledge one possesses.

And, finally, to the world, the chaotic stream of order in which everything that encapsulates all of us resides.

"The opposite of every truth is just as true."
(Hermann Hesse)

Abstract

The current dissertation focuses on the development and improvement of a numerical model, with its main objective being the simulation of the mechanical behaviour of a railway section, specifically on the simulation of track responses to quasi-static loads. The definition of modelling parameters is made upon the reduction of the difference between numerical and experimental responses. This was done by, firstly, developing a finite element model and bettering its responses by using a Design of experiments framework and Monte Carlo simulations to adapt the parameters. Secondly, in order to study the influence of a geosynthetic on the model, the behaviour of the model with, and without, the addition of a geogrid was also studied. The behaviour of the numerical model was closely approximated to that of the experimental model and the influence of the geogrid proved to be substantial due to the compaction in the elements close to it.

This study is a step towards the development and implementation of techniques to improve the evaluation of the mechanical performance of railways by making use of the experimental measurement and numerical simulations by focusing on localizing track sections which need inspection and maintenance operations.

Keywords: Railway, Numerical Model, Geogrid, Mechanical properties, Design of Experiments

Resumo

A presente dissertação foca-se no desenvolvimento e melhoria de um modelo numérico, tendo como principal objetivo a simulação do comportamento mecânico de uma secção de uma ferrovia, mais concretamente a emulação das respostas à aplicação de cargas quasi-estáticas. A definição dos parâmetros de modelação é desenvolvida através da redução da diferença entre as repostas do modelo numérico e experimental. Isto foi atingido com, em primeiro lugar, o desenvolvimento de um modelo de elementos finitos e a melhoria das suas respostas através do uso da metodologia de *Design of experiments* e do método de *Monte Carlo*. Em segundo lugar, de forma a estudar a influência de geosintéticos no modelo, o comportamento com e sem a adição de uma geogrelha também foi estudado. O comportamento do modelo numérico foi aproximado ao do modelo experimental e a influencia da geogrelha provou ser substancial devido à compactação nos elementos em contacto com a mesma.

Este estudo é um passo na direção do desenvolvimento e implementação de técnicas para melhorar a avaliação do comportamento mecânico de ferrovias através do uso de medições experimentais e simulações numéricas através do foco em localizar secções da via que necessitam de inspeções ou operações de manutenção.

Palavras-chave: Ferrovia, Modelo numérico, Geogrelha, Propriedades mecânicas, *Design of experiments*

Contents

List of Figures

List of Tables

Glossary

Ballast Breakage Index Ballast breakage index (BBI) is a measure of the physical degradation of ballast, which is the crushed stone or gravel material that forms the foundation of a railway track. It is defined as the percentage of the total weight of ballast that is reduced to smaller sizes due to crushing or grinding during the service life of the track. A high BBI value indicates that the ballast has experienced significant degradation and may need to be replaced in order to maintain the structural integrity and stability of the track. *(pp. 5, 6, 25)*

Design of Experiments Design of experiments (DOE) is a method for planning and conducting experiments to optimize the relationship between input variables and output variables. It involves manipulating input variables according to a predetermined plan and measuring the corresponding responses in order to identify and optimize the relationship between the variables. It is often used to improve the efficiency, effectiveness, and robustness of a process or system. *(pp. 35, 41, 51)*

Finite Element Method The finite element method (FEM) is a numerical method used to solve differential equations that describe the behavior of physical systems. It involves dividing the system into small elements and solving equations defined at the nodes, which are connected by the elements. The method is widely used in engineering and applied mathematics to analyze complex systems and is particularly well suited for problems involving large deformations and time-dependent behavior. *(p. 11)*

Friction angle In the context of this thesis, the friction angle is a measure of the resistance to sliding between two rocks that are in contact with each other. It is a property of the materials of the surfaces and is related to their inherent frictional characteristics. The friction angle is defined as the angle of repose, which is the maximum angle at which a slope made up of a particular material will remain stable without sliding. *(pp. 5, 26, 49, 50, 55, 56)*

Monte Carlo method The Monte Carlo method is a computational algorithm that relies on random sampling to obtain numerical results. It is often used to solve mathematical problems that cannot be solved analytically, or to estimate the probability of certain events occurring. The basic idea behind the Monte Carlo method is to use random sampling to obtain a set of possible outcomes for a given problem, and then use the results of those samples to estimate the probability of different events occurring or to compute a numerical result. *(pp. xii, 17, 22, 44, 45)*

Static analysis A static analysis with the finite element method is a numerical method used to solve differential equations that describe the behavior of a physical system under quasi-static (i.e., non-dynamic) conditions under a fictitious time. In a static analysis, the system is subjected to a fixed set of loads and boundary conditions, and the goal is to determine the resulting displacement and stress distribution within the system. In this dissertation, the tests are run using *ANSYS APDL* software. *(pp. 24, 27, 35)*

Acronyms

RMR Regression Model Representation *(pp. 17, 18, 21, 41–43, 46, 47)*

RS Response Surface *(pp. 17, 22, 44)*

Symbols

A	Cross section area *(p. 32)*
δ	Physical deformation of a longitudinal spring *(p. 32)*
E	Young modulus *(pp. 32, 46, 51)*
G	Shear modulus *(p. 33)*
I	Moment of inertia *(p. 32)*
K	Spring constant *(p. 32)*
L	Length *(p. 32)*
$\mathbf{M_{Oed}}$	Oedometric Modulus *(p. 34)*
ν	Poisson's ratio *(p. 33)*
ρ	Density *(p. 33)*
σ	Normal stress *(pp. 12, 32)*
τ	Tangential stress *(p. 12)*
ε	Strain *(p. 32)*
ζ	Physical deformation of a rotational spring *(p. 33)*

1

Introduction

1.1 Motivation

With the current ecological development of the planet, and the urgency to improve it [2], the means of transportation with a smaller ecological footprint are becoming increasingly important, so it is necessary to develop more, not only rail transport, but also all other means in order to create a network capable of reducing dependence on transport with a combustion engine. Taking into account the monetary, time and resource costs that periodic inspections of tracks tend to have, together with the absence of a way of predicting the behavior of sections of the tracks, the inspection of the railways can become impractical and lead to errors that would otherwise be avoidable [3].

Recent studies, although already well developed in the scope of numerical modeling of railways, do not tend to take into account the addition of geogrids (section 1.2.2.1), and are quite specific regarding the situation in which they are applied instead of taking a parametric approach in order to facilitate the application of the model in different situations. As such, the present investigation aims to present an approach where, through numerical modeling with finite elements, it is possible to analyze a section of a railway and the effect caused by the presence of a geogrid, therefore complementing the development of the area from the railway. This is done with a specific focus on the development a computational model which enables the evaluation of a track section by aiming at the resemblance of experimental and simulated track courses.

1.1.1 Objectives

The dissertation shall aim to develop a highly parametric numerical model capable of simulating the behavior of a real-life railway track in various situations. The numerical model will be further developed in *ANSYS APDL* and *Matlab* softwares simultaneously, and use the Finite Element Method to approximate the behavior of a section of the railway track in most circumstances it is meant to analyze. Meanwhile, there will be a deepening of the study of geogrids and their influence on the track, as well as their pros and cons in this regard.

1.1.2 Dissertation Layout

Along with the current chapter, there are a total of five chapters. With this chapter being an introduction to the dissertation, including an introduction to the concept of a geogrid and its uses, overall study of some of the most important modern introductions to the classic railway track, from elastic to non-elastic elements (section 1.2), with a deeper focus on the geogrid. It also encapsulates the parameters that are base of monitoring modern railways.

The second chapter is a presentation of several studies which encapsulate the working of the numerical and experimental model. Focusing on the criterion of deformation, hardening rule and types of elements (in the *ANSYS APDL* software), overview of experimental studies and Design of experiments.

Chapter 3 leans over the development of the numerical model, justifying the choices made for the geometry and each section of the numerical railway, as well as the boundary conditions for each section. It also presents the initial choices for physical properties for the model.

In the fourth chapter, the process of choosing the best values for physical properties, when comparing to the experimental study, as well as the analysis of the results after setting the geogrid within the numerical model of the railway is presented.

The final chapter includes the conclusions made of the work developed in this dissertation, as well as propositions for future advances in this research.

1.1.3 Geogrid

Geosynthetics have an increasingly important role when it comes to stabilizing and reinforcing structures in various applications. This increase has resulted in a dynamic upsurge, not only in applications, but also in types of geosynthetics available for use and, because of that, new geosynthetics have been developed in order to increase their range of applications, thus the geogrid was created and applied in railways (among other structures, like walls or soils).

Usually composed of polyethylene (HDPE) or polyester (sometimes recycled), when put in a mechanism where stabilization is the basic necessity, the changes created due to the addition of a geogrid tend to be the following [4]:

- Mechanical stabilization of subgrade and structural layers of roads, railway lines, runways, among others;
- Stabilization of working platform layers;
- Stabilization of floor bases;
- Stabilization of the toe of embankment, max. 2.5 m high, formed on a soft soil;
- Geosynthetic protections in the mining and seismic areas;

- Stabilization of aggregate pad layers - geo-mattresses.

There are three main types of geogrids, used in different types of applications. The uniaxial geogrid, the biaxial geogrid and the triaxial geogrid. Each axial direction is a direction for which the geogrid offers support [5].

1.1.3.1 Uniaxial geogrid

A uniaxial geogrid (figure 1.1) is a type of geosynthetic material that is commonly used in civil engineering and construction projects. It consists of a series of closely spaced, parallel ribs that are interconnected by a network of integral junctions. The primary function of a uniaxial geogrid is to provide reinforcement and stabilization to soil structures.

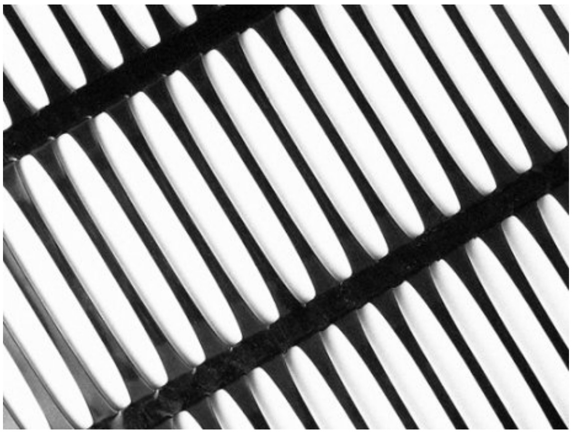

Figure 1.1: Uniaxial geogrid [5].

Uniaxial geogrids are typically used in applications such as embankments, retaining walls, bridge abutments, and roadways. They are designed to improve the strength and stability of these structures by distributing the load and reducing the stresses placed on the underlying soil. In addition, uniaxial geogrids can help to minimize the amount of fill material required for construction projects, which can result in significant cost savings.

1.1.3.2 Biaxial geogrid

Biaxial geogrids (figure 1.2) are commonly used in a variety of civil engineering applications, including soil reinforcement, slope stabilization, and retaining walls. The main advantage of biaxial geogrids over uniaxial geogrids is that they provide equal strength in both the longitudinal and transverse directions. This allows them to withstand multidirectional stress and deformation, making them ideal for applications where there is not a single dominant stress direction.

Additionally, biaxial geogrids are more flexible and conformable than their uniaxial counterparts, allowing them to be used on irregular surfaces without losing their reinforcing capabilities. Biaxial geogrids are often made from materials such as high-density polyethylene (HDPE) or polyester, and are designed to resist environmental factors such

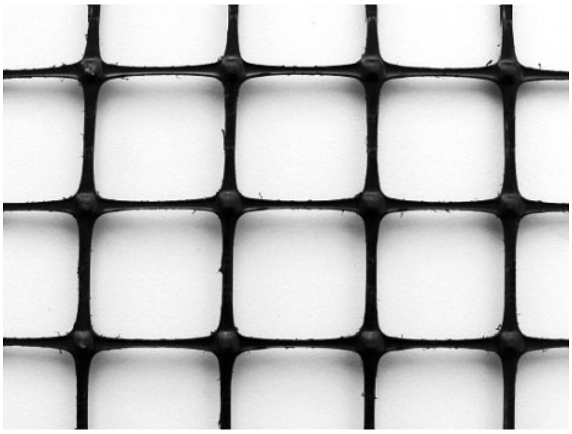

Figure 1.2: Biaxial geogrid [5].

as ultraviolet radiation and chemical exposure. Overall, biaxial geogrids are a versatile and effective solution for a wide range of civil engineering challenges.

1.1.3.3 Triaxial geogrid

A triaxial geogrid (figure 1.3) is a three-dimensional geosynthetic material that provides reinforcement in all three directions. Triaxial geogrids are commonly used in applications where there is a need for significant reinforcement in all three directions, such as in road and railway construction. They are particularly useful in areas with poor soil conditions, where they can improve stability, reduce deformation and increase the load-bearing capacity of the subgrade.

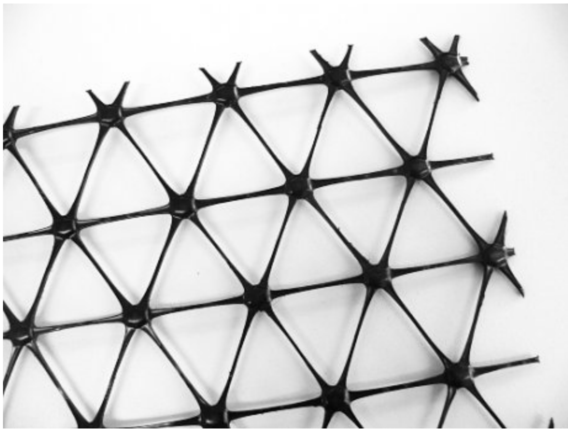

Figure 1.3: Triaxial geogrid [5].

The use of triaxial geogrids can also reduce the amount of excavation required, which can lead to cost savings and a reduction in environmental impact. Additionally, they can be used in slope stabilization, retaining wall construction, and embankment reinforcement. The unique properties of triaxial geogrids make them an ideal choice for a range of civil engineering applications.

Thus, these types of progression are what is to be expected when a geogrid is applied to a railway. The use of geogrids has several upsides when it comes to construction and hard maintenance interventions in railways. The presence of a geogrid in between the ballast and sub-ballast (figure 1.4) of a railway increases the lateral resistance of the track (but only in the areas close to the geogrid [6]), thus diminishing settlement and increasing time in between maintenance interventions. When a geogrid is applied to the track, the natural friction in between the rocks composing the ballast, known as Friction angle, no longer is the only mechanism resisting settlement, as the existing traction within the geogrid increases significantly the Friction angle which, in turn, increments the resistance, hence the settlement, Ballast Breakage Index and minimum initial ballast layer thickness diminish significantly [2, 7, 8].

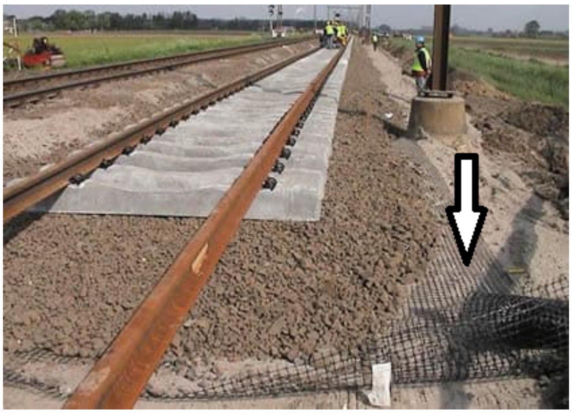

Figure 1.4: Placement of a geogrid between the sub-ballast and the ballast. [9].

1.2 Modern Ballasted Railway

The ballasted railway track (figure 1.5) is the most common railway in the world and, as expected, there have always been changes to try and improve it. In the modern age, trains have gotten more normalized, cheaper and faster, so improving the tracks is not only a step towards evolution but it's also a very real necessity. Consequently, methods of improvement have been put in place to make the railways more durable, stable and cheaper to build and maintain. Some of those methods will be the focus of the study.

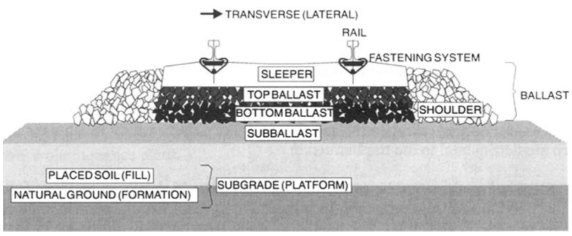

Figure 1.5: Ballasted Railway Track and its components [10].

Given the long story of railway transportation (starting in the age of enlightenment), railways have shifted and evolved to the point where they are today and there are new innovations being implemented and brought to light in order to keep them relevant and capable of facing a world in a fast pace of change. The main methods implemented in ballasted railways in order to decrease geometry degradation - due to ballast settlement and particle breakage - are: elastic elements, geogrids and bituminous layers [11].

1.2.1 Elastic Elements

The three main approaches used when it comes to the application of elastic elements in order to decrease ballast settlement are: the use of softer rail pads, in an attempt to decrease the pressure and vibration applied on the sleepers; the use of under sleeper pads, where by applying a pad under the sleepers, the vibrations transmitted to the ballast are significantly decreased and, therefore, the settlement diminishes; there is also the under ballast mat, which is mostly used in specified circumstances, otherwise having mixed results [11].

1.2.1.1 Rail Pads

Although rail pads with high stiffness tend to often used in railways for high-speed lines, softer pads allow for a reduction in vibration caused by anti resonance that, in return, transmits vibrations and loads in a more severe manner, thus damaging, not only the ballasts, but also the rails and sleepers. Although this approach is better for the structure, softer pads tend to require maintenance more often, as they usually wear out sooner [12, 13].

1.2.1.2 Under Sleeper Pads

Under sleeper pads are pads that are applied under the sleepers with the intent to diminish the settlement by reducing the existing stress at the sleeper-ballast interface, thus decreasing the Ballast Breakage Index and stiffness. With the application of softer pads, the stress is reduced to an even greater extent which will, consequently, result in less wear on the ballast [7, 11, 14].

1.2.1.3 Under Ballast Mat

Although it may be applied very much in the same way that a bituminous layer might be, it does not fit the same way nor does it have the same characteristics. When an under ballast mat is used in a track, the main change in performance is the lower transmission of the vibrations from the ballast to the sub-ballast and, even though it is less normalized, the mat may as well be applied under the sub-ballast. The under ballast mat can be either stiff or soft, resulting in a variation in track displacement and vibration transmitting, with higher stiffness being associated with lower displacement (and amplitude) and more vibration transmission. The presence of an under ballast mat also creates a variation in the train-track interaction, which is the result of the change in the response present in the ballast [8, 11, 15].

1.2.2 Non-elastic Elements

The non-elastic elements are additions to the railway whose approach does not incorporate the mitigation of vibration in its modus operandi. In this case, the bituminous layer and the geogrid are the non-elastic elements presented.

1.2.2.1 Geogrids

A geogrid is a commonly used material in railway construction due to its ability to improve the stability and load-bearing capacity of the railway. Their use helps to reduce the risk of track settlement and improve the overall performance of the railway. When installed beneath the ballast layer, geogrids act as a stabilizing layer that spreads the load of the train across a larger area, reducing the stresses on the subgrade soil.

Geogrids can be used in both the construction of new railway lines and the maintenance of existing ones. In new construction, they are installed before the ballast layer, while in maintenance, they can be added to the existing ballast layer. In both cases, the geogrid helps to prevent the ballast from sinking into the subgrade soil, which can lead to track deformation, loss of alignment, and even derailment.

Furthermore, geogrids can also be used in conjunction with other track stabilization methods, such as geotextiles and drainage systems. The combination of these methods creates a more resilient track structure that can withstand heavy loads and extreme weather conditions.

The use of geogrids in railways has proven to be an effective way to improve track stability and reduce maintenance costs [6, 16]. With the growing demand for efficient and reliable railway transportation, geogrids are likely to become an increasingly important component in railway construction and maintenance.

1.2.2.2 Bituminous Layers

Although requiring a significantly higher investment cost, applying a bituminous sub-ballast layer will decrease the pressure and dynamic forces created by the passage of trains whilst also preventing the infiltration of water into the substructure. It also plays a role in decreasing vibration transmission to the sub-structure (to a lower degree than the under ballast mat) and, because of that, the maintenance cost shall decrease significantly and the money will most likely be made back in up to 7 years [11, 17].

While there are very important advantages in the use of a bituminous sub-layer, the temperature is an issue that can be problematic, as the increase in temperature can affect the resistance to punching and plastic deformations. Even so, there have been developed methods to counter these situations, mostly the presence of ballast serves as heat insulator, thus decreasing the thermal amplitude influencing the bituminous layer [3, 18, 19].

1.3 Parameters of Monitoring

Railway monitoring is a complex field of study, as it has several approaches and ways of monitoring. Nonetheless, it's been admitted to be two main groups of measurable parameters when it comes to track conditioning [20].

The first method is based on the deterioration of each component of the track, where the main parameters of analysis are the changes that each component is subject to as time goes on and the track is used. The second method, the one which most machines tend to measure, has a different approach, where the main focus of monitoring is the evolution of the rail tracks geometrical properties (which, in later stages, becomes degradation) caused by the continuous strain the track is subject to over time [20–23].

In the case of a numerical model, the first method (the deterioration of each component) cannot be accurately measured by a unique descriptor, as those tend to vary widely with very specific conditions (such as rain, wind or oxidation, for example) that aren't possible to account for with this kind of model. Therefore, the only degradation examined with the numerical simulation will be the geometrical (the second method).

1.3.1 Measured Parameters

Portuguese railways use the Plasser & Theurer EM120 equipment as the main railway measuring tool. Given that, the parameters measured by the EM120 machine shall be the ones presented in this section. The parameters that the equipment is capable of measuring are: longitudinal profile, horizontal alignment, gauge, superelevation (Cant irregularities) and loaded gauge (which is the distance between the rails when load is applied) as shown in figure 1.6 [23, 24].

Although there are several measuring parameters to analyse the status of a railway, when developing a numerical model, there are a few limitations in the model to be developed, such as the need for symmetry (which makes it not possible to account for Cant) and, with the application of purely vertical loads, the alignment and gauge of the rails will also not be accounted for. So, in the current dissertation, the longitudinal level is the main parameter that the model can accurately measure. But, although only the longitudinal level is measured, a 2D model would not have an approximation as viable as the 3D model. This is because a 3D model provides a more realistic and comprehensive representation of the physical system being modelled, while in 2D modelling, the system is represented as a flat plane, which means that certain aspects of the system, such as depth and height, cannot be accurately represented. When the system is as complex as a railway, these parameters become increasingly important.

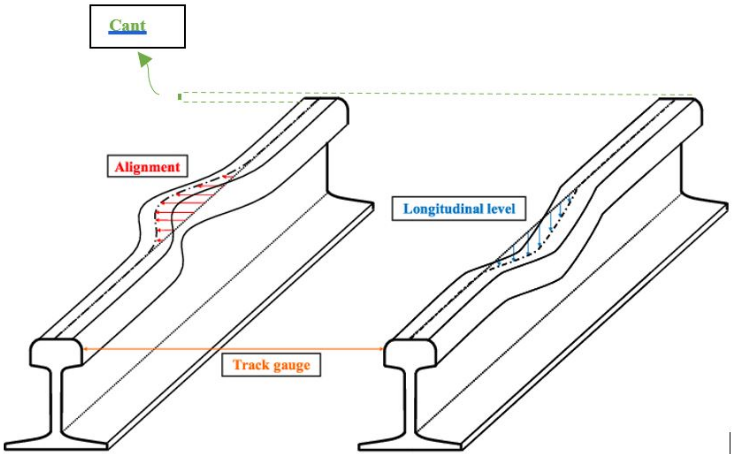

Figure 1.6: Measured parameters (Loaded gauge isn't represented) - adapted from [25].

Longitudinal Profile

The longitudinal profile mostly handles the vertical displacement and amplitude (the difference between the displacement with and without load applied) created in a track after repeated use. The vertical displacement is catalyzed by vertical loads (dynamic and static) applied continuously to the track, changing gradually the vertical geometry of it through plastic deformation, as seen in the figure 1.7 [25, 26].

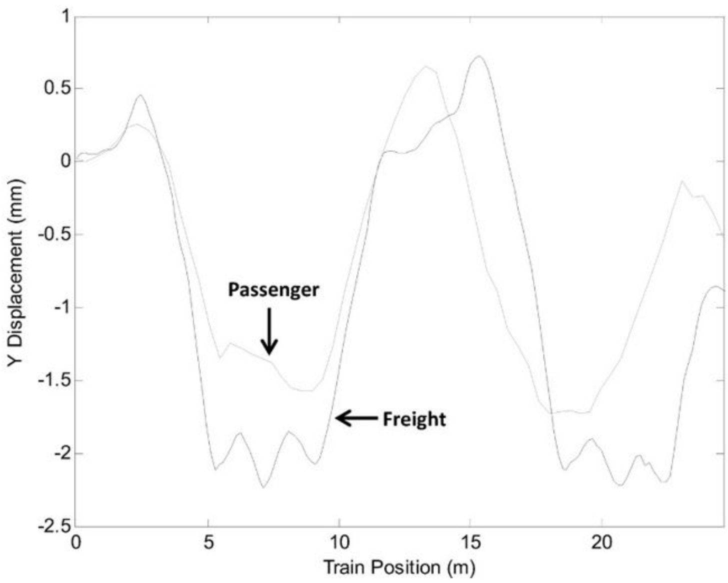

Figure 1.7: Short-term vertical reaction of the track after different types of trains pass on it. Noticing the elevation above nominal value after the application of loads [26].

The reason why there's an elevation after the force is applied (figure 1.7) by the trains is - by Newtons third law - since the subgrade creates tension to support the train, when the force ceases, there's a reaction of the subgrade, resulting in the elevation of the rail above the previous nominal value.

Horizontal Alignment

Irregularities in the horizontal alignment are deviations from the nominal track center. These irregularities are capable of causing very complicated and uncomfortable vibrations, which can, in a worst-case scenario, cause catastrophic accidents [27]. The main reasons for these irregularities tend to be the lateral component of friction between wheel and rail; uncompensated centrifugal acceleration; geometrical variation due to temperature oscillation caused by bending instigated by longitudinal forces, usually derived of the acceleration of vehicles.

Track gauge

The smallest distance between the inside of the two rails, usually measured within 14 mm below the running surface is the track gauge. The deviation from the nominal value is known as a track gauge irregularity. Although the standard track gauge is 1435 mm, in the Iberian Peninsula it's 1668 mm [27, 28].

Cant

Cant is the comparison in height between the height of the rails at their highest point. When there's an unintentional rotation of the track around its longitudinal axis, there's a difference in height between both rails, it is known as a superelevation (or Cant irregularity) [27].

2

Theoretical survey

The ballasted railway has been subject to several studies and changes over the years. With the ever-increasing need for more, faster and tougher railway transportation, with higher performances and lower costs, the method of construction and maintenance has to be on par with the requirements of modern society, especially with the increased inter connectivity between countries and civilizations.

When it comes to the maintenance of existing railways, there are three main approaches. The first one is based off of in field studies and analysis where, by using a specialized vehicle, it is possible to deeply analyze the track (for example, the EM120 machine); the second method is by using laboratory models where, by emulating the conditions and applying loads similar to what the track in question is subject to, the results are expected to be similar to what will happen in the railway; the third, and final, approach is the one that will be developed and studied in this dissertation, which is the numerical model, a method used to simulate, with the use of modern software and hardware, the behaviour of a railway track.

As for the numerical model, there are various ways to approach the problem, the one used in this dissertation used a 3D numerical model and made use of Finite Element Method (FEM) to study the behavior of the railway with and without the presence of a geogrid, in order to assess its influence within a numerical model. This analysis shall be done with *ANSYS APDL* and *Matlab* simultaneously in order to compare the results and obtain the best model possible.

2.1 Plastic deformation

The relation between the magnitude of applied loads and the resultant strain is the function of the mechanical properties of the material. There are different criteria which were developed in order to, mathematically, predict the behavior of a body when subject to certain conditions.

When it comes to yielding, there are different criteria used to indicate when a body will enter plastic deformation and these have a very important role in dictating the way the body behaves when non-linear deformation takes place.

2.1.1 Von Mises criterion

The von Mises criterion (equation 2.1, written for the Cartesian coordinate system; adapted from [29]), used in *ANSYS APDL* software, is the yield criterion based in the maximum distortion energy applied into the material on question, it is mostly applied in materials that tend to be ductile. When the coordinates (stresses) reach the surface of the "cylinder"(Figure 2.1), the body reaches yield stress.

With σ being the stress applied in the direction of each axil, normal stress; τ, the shear stress and Sy representing von Mises stress applied to the material.

$$S_Y = \sqrt{\frac{(\sigma_1 - \sigma_2)^2 + (\sigma_2 - \sigma_3)^2 + (\sigma_3 - \sigma_1)^2 + (\tau_{12}^2 + \tau_{23}^2 + \tau_{13}^2)}{2}} \quad (2.1)$$

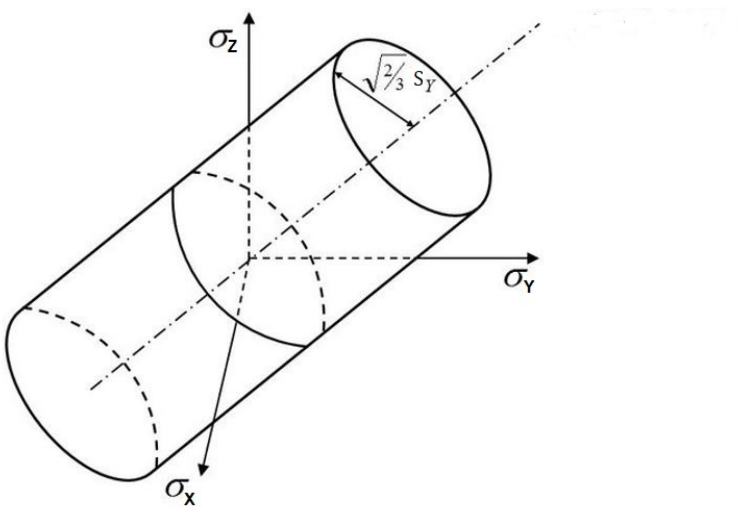

Figure 2.1: Geometrical representation of the Von Mises criterion in 3D [30].

If S_Y is greater than the simple tension yield limit, as shown in equation 2.1, then it is expected for the material to yield. Even though the Von Mises stress is not a true stress, it is a theoretical value that serves as a benchmark that allows for better knowledge when calculating real values of yield stress [29].

2.1.2 Hardening Rule

Plastic deformation is, to this day, still an active field of study due to the limitations the current widely used hardening rules still have when applied to the, increasingly complex, engineering challenges of the modern age. Thus, when choosing a hardening rule to apply for a specific analysis, in this case the FEM, an analysis needs to be made of the rule to be chosen, as not only the rule, but the way it's applied has relevance in the results obtained.

The type of hardening rule applied in the development of the dissertation is the bilinear isotropic hardening (figure 2.2). Multilinear isotropic hardening is not applied in this dissertation because the sections that compose the railway, although they are different from each other, are not composits, as the grains that each section are of the same material and similar in shape and size, thus each section starts to deform permanently, and evenly, when under the same yield tension [31]. Bilinear hardening is defined by the direct transition from elastic to plastic deformation and by the uniform way the yield surface expands (or shrinks) about the hydrostatic axis, as shown in the figure 2.3(a).

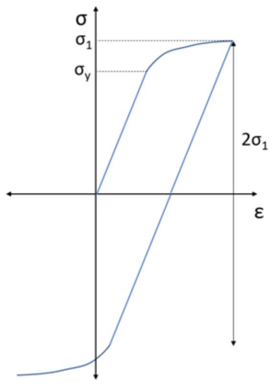

Figure 2.2: Isotropic stress-strain relation [32].

The isotropic model, differing from the kinematic model (figure 2.3(b)), does not account for the *Bauschinger effect*, which is defined by the combination of the permanent strain hardening and residual stresses that the material will acquire as it flows, but, since the loads applied in the structure are always cyclical and in the same direction, there is no need for the application of the *Bauschinger effect*, hence the isotropic model being a viable option in this case [31].

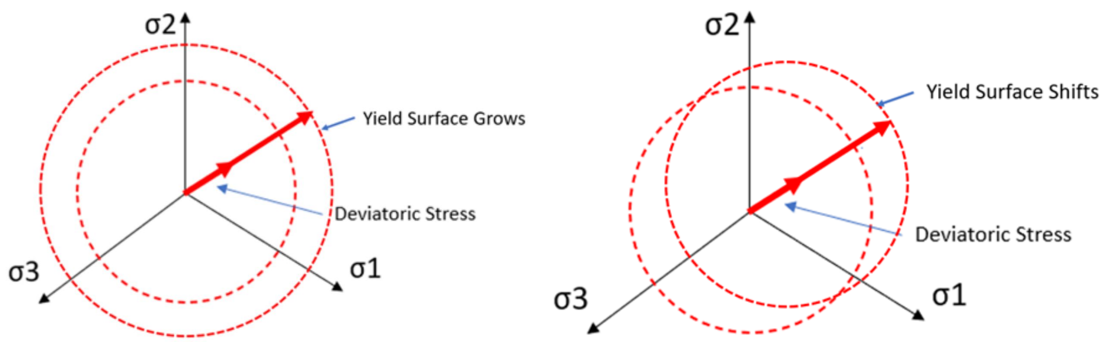

(a) Isotropic yield surface evolution (b) Kinematic yield surface evolution

Figure 2.3: Isotropic and kinematic behaviours [32].

2.2 Elements (ANSYS APDL)

When working with *ANSYS APDL*, in order to create the closest approximations possible, there are hundreds of different element types, each with a specific purpose (even though some are able to emulate similarly well when under some of the same conditions).

The four element types chosen to be used in the development of the numerical model are [33]:

- BEAM188 - Rails;
- SOLID185 - Sleepers, ballast, sub-ballast and foundation;
- COMBIN14 - Rail pads and elastic boundary conditions;
- SHELL181 - geogrid;

2.2.1 BEAM188

Designed to model slender to moderately thick beam structures, the BEAM188 (figure 2.4) is a "linear, quadratic, or cubic two-node beam element". Making use of the Timoshenko beam theory in order to account for shear deformation effects, it has six or seven degrees of freedom per node (with translations along and around the x, y and z axles, accounting for six degrees of freedom. With the possibility to add warping effect, increasing the number of degrees of freedom to seven).

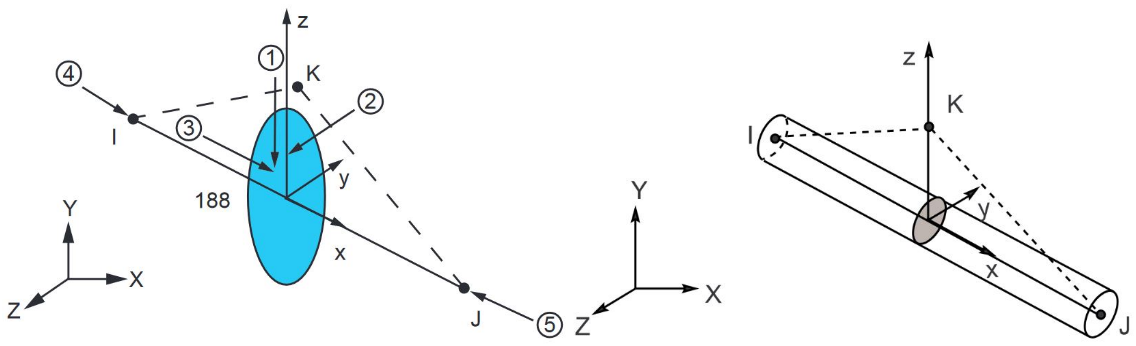

(a) BEAM188 beam element (b) Representation of a 3D beam element

Figure 2.4: Illustration of the BEAM188 element [34].

With the option of large deflection, stress stiffness is also included, thus making it possible to analyze flexural, lateral and torsional stability problems. It also allows for a diverse amount of shapes of cross sections, making it possible to create several types of cross sections with highly approximate calculations of parameters of the beam, one of those being moment of inertia [34].

2.2.2 SOLID185

The SOLID185 (figure 2.5) was developed with the intention of modeling solid 3D structures, making use of 8 nodes per element, each with three degrees of freedom, those being the translations in the directions of the x, y and z directions, with orthotropic behaviour.

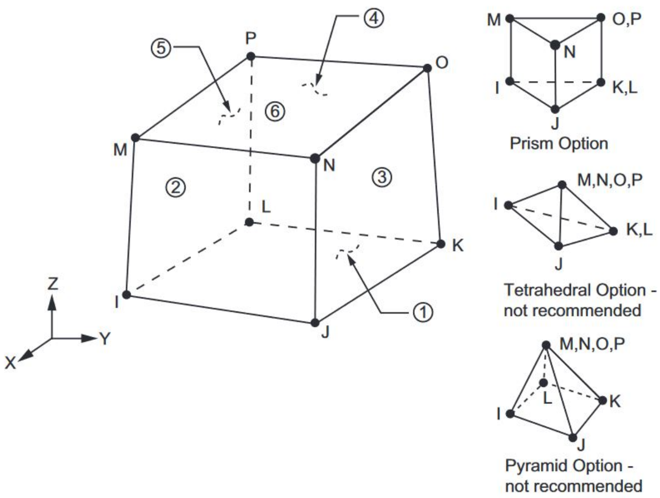

Figure 2.5: Representation of the SOLID185 element [35].

Being a complex element, it allows for the use of hyper elasticity, stress stiffening, creep, large deflection and large strain capabilities. Even though not all of these are used in the model, they are representative of the high level of adaptability that this element has. The effects of pressure load stiffness are also accounted for, even though they are primarily defined as symmetrical, this is also possible to change if needed [35].

2.2.3 COMBIN14

The COMBIN14 (figure 2.6) is an element without mass, with longitudinal and/or torsional capabilities in all three dimensions, being able to emulate either springs and/or dampers. Each node has three degrees of freedom, either rotational or longitudinal, around or translating along the x, y and z axles, respectively. It's composed of two nodes, one for the spring constant and another for both damping coefficients (one for the constant damping coefficient and the other for the nonlinear damping effect, which tends to act in some fluids).

It's possible to add preloads to the springs in one of two ways, either by adding an initial force to the spring or an initial increase, or decrease, in length (that being either torsional or longitudinal). The spring constant relates the force with length or radians, depending on whether its a longitudinal or torsional spring, while the damping is defined by the relation of force times time divided by length or radian, for longitudinal and torsional, respectively.

When modelling with the use of COMBIN14, the x, y and z axles are automatically aligned with the global coordinate directions, but, when necessary, it's possible to change

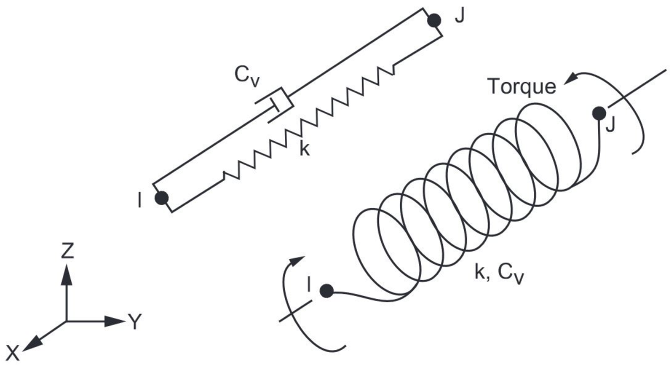

Figure 2.6: Illustration of longitudinal and rotational spring (k) and damper (C_v) [36].

the coordinates in order to accommodate the situation that requires it [36].

2.2.4 SHELL181

The SHELL181 (figure 2.7) is used as an element type developed to analyse shell structures, usually from thin to moderately thick. Each element is composed of four nodes, each with six degrees of freedom (three of translation in the direction of the x, y and z axles and three torsional around the same axles), but, when the membrane option is applied, the torsional component to the nodes ceases to be regarded.

Being specialized for linear, large rotation and/or non linear application, even the change in shell thickness is accounted for when under non-linear analysis. This is also the case with the load stiffness derived from distributed pressures.

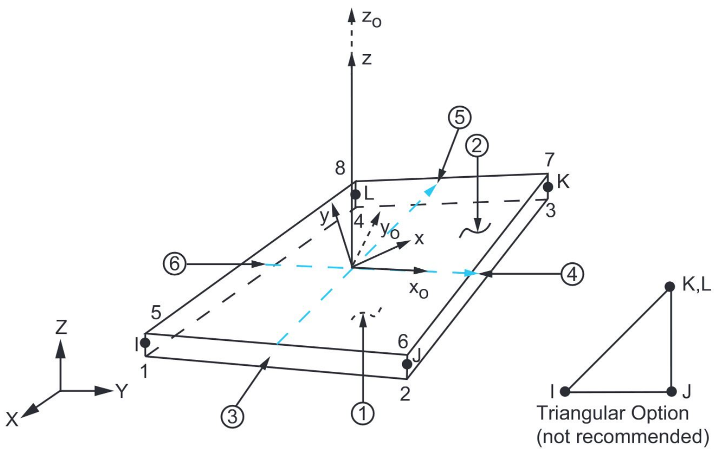

Figure 2.7: Illustration of the SHELL181 element [37].

When designing composites, it's possible to create models with different layers, known as sandwich construction. This type of model is governed by the first order shear deformation theory (Mindlin-Reissner shell theory). The kinematics of the element, by making use of logarithmic strain and true stress measures, allows for stretching (which is the finite membrane strains). But the time increment is assumed to be small on order for this to be applied [37].

When studying a structure as complex as the numerical model presented, the properties for each element have an influence over the overall behaviour of the railway. Thus, when performing analysis where, not only the final result, but also the optimal values and combinations for input variables (as well as the relationship between them) are unknown, the use of a systematic method for planning and conducting experiments is of use.

2.3 Design of experiments

In order to develop a study dependent on two or more factors, especially when these factors are meant to be combined with the objective of obtaining an optimal result, there needs to be an experimental approach, allowing for the analysis of the effects that, not only each parameter directly has, but also the interactions between them have on the result.

In the first stage of design, a 2^k factorial design is one of the mainstream approaches used in order to identify the tendency in which the factors tend to change as the results get closer to the objective, with **k** being the number of factors. With this, not only is a close value to each parameter obtained, but a Regression Model Representation (RMR) is derived with the use of the effects calculated in the best combination of parameters, allowing for, not only the ability calculate the response of each test, but also to create a surface response in order to predict the response with various combinations of design factors when the values for each factor don't stray too much away from the interval used in the 2^k factorial design [38].

After the factorial design is run, there is need to further lower the error of the model. With the use of the RMR and Response Surface (RS), an approximation to the optimal value for each parameter (closing the existing gap due to the limitations of the 2^k factorial design) is calculated through an adjusting process. In which the approximate results derived from the 2^k factorial design are then adjusted through the use of the calculated effects of the parameters (by the usage of the RMR), ensuing in a much more accurate (although not exact) result. This is done by applying the Monte Carlo method.

After the RMR is calculated, the optimal model needs to be obtained, but, when there are more factors than equations at play, it is not practical to obtain an optimal solution without a statistical method. In this problem, the chosen method of adjustment was the Monte Carlo method, which, by randomly generating uniformly distributed numbers within a pre-defined domain enough times (by making use of the law of large numbers) various approximations to the optimal solution are generated. When this process is run enough times and the solutions converge so a certain value, a viable approximation is achieved by making an average of all the solutions with the lowest error (or euclidean norm of the errors, when there are multiple solutions).

2.3.1 2^k factorial

In the first phase of an experiment, when there isn't much information about how the results of a parametric model are influenced by a quantitative/qualitative change of each (or combination of) factor(s), there needs to be an initial stage where it's possible to study the tendency of the results in a fast and efficient way, whilst analyzing the effect that a change in a parameter has on the results, known as main effect, and the effect that exists according to each combination of factors, known as interaction. This method of experimentation is very useful in this situation because, with every complete trial, there is an analysis of every possible combination, which allows for a complete investigation of the problem [38].

The 2^k factorial design is applied in the following way:

1. The factors which are to undergo changes and analysis are defined;
2. There are two levels that are chosen for each factor;
    - Two levels of values are defined, usually named "high" and "low" or similar;
3. For each change in level a test is run, with the objective of analyzing every possible combination in order to study the changes in results;
4. With the use of the complete set of tests, the main and interaction effects are calculated;
5. A RMR is written with the use of the results and effects previously obtained;
6. Adjusting the model.

One of the reasons why the factorial design is important is the efficiency with which it works and is applied on experiments. Each factor (quantitative or qualitative) can only have two levels, which allows for an in-depth study of the response of the experiment by studying every possible combination of both levels of parameters, allowing for an accurate estimation of the effects of a factor at both levels while avoiding misleading conclusions.

When using factorial design, there are a few important rules that must be known beforehand. Firstly, the effect of the parameters has to be unidirectional because, if it's not, the interaction can become unreliable, since the crossed effect can be much lower, or higher, than the actual effect of the factors. Secondly, by only having two levels for each factor, the amount of testing (and cost) necessary for analysis is severely lowered, but it also limits the process, as it needs to be adjusted afterwards by making use of the RMR and response surface to obtain accurate values [38].

In this example, the aim will be to obtain 65 as a result. Using an example of a 2^2 factorial design (table 2.1) since, regardless of the number of factors, the method of application is similar:

Table 2.1: Example of experiment, with values for each level of A and B.

	B1	**B2**
A1	25	55
A2	47	80

Table 2.2: Levels for each factor.

A	-1, for A1 1, for A2
B	-1, for B1 1, for B2

Each, as stated, factor has two levels (table 2.2):

The tests run can be counted and identified by making use of a square scheme - figure 2.8 - (allowing for a visual representation of the study) and sign table - 2.3 - (showing which combinations are made in the set of experiments), in which each combination of tests is represented, counting the interaction. These two approaches work together in representing the process.

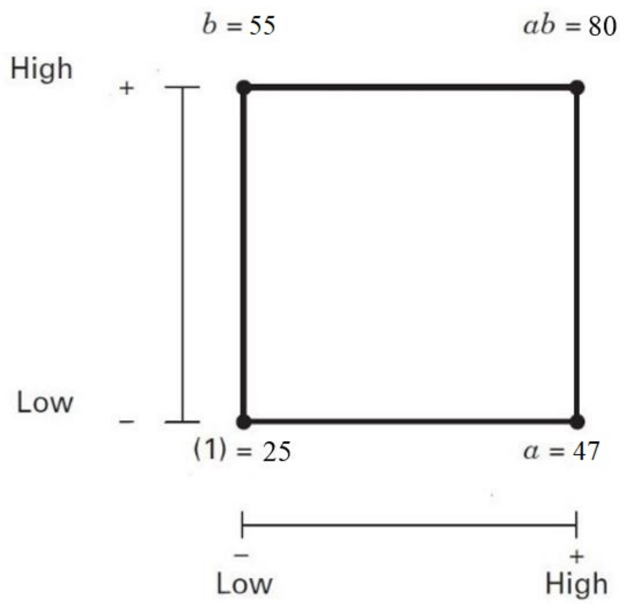

Figure 2.8: Combination of the design. Adapted from [38].

The usual nomenclature for the response of each test is represented in table 2.3, with **a** representing the combination of A at high level and B at low level, **b** representing A at low level and B at high level, **ab** with both factors at high level and **(1)** with both at low level. This is referred to as standard order. The **I** column is the identity element, and its main use is to find out the grand sum of all possibilities.

The contrast is usually known as the *total* effect of a factor, and is obtained using equation 2.2. It relates to the effects, main and interaction. The sign in each set of

Table 2.3: Sign table.

	Factorial Effect			
Treatment combination	I	A	B	AB
(1)	+1	-1	-1	+1
a	+1	+1	-1	-1
b	+1	-1	+1	-1
ab	+1	+1	+1	+1

parameters is negative if the factor is at level "high"in the effect and negative if otherwise, while the (1) is changed to just “1”.

$$Cons_{AB...K} = (a \pm 1)(b \pm 1)\ldots(k \pm 1) \tag{2.2}$$

Applying it to the example for each factor,

$$Cons_A = (a - 1)(b + 1) = ab + a - b - (1) \tag{2.3}$$

$$Cons_B = (a + 1)(b - 1) = ab + b - a - (1) \tag{2.4}$$

$$Cons_{AB} = (a - 1)(b - 1) = ab + (1) - a - b \tag{2.5}$$

As stated earlier, the effect of a factor is the change in the produced response by a change in the level of a factor and, although it’s not the case in the current example, experimental tests can have changes in results when they’re not run through computational methods. Thus, there might arise the need to run more than one test for each combination of levels and then use the average results as a basis for the analysis. The number of tests (replicates) taken for each combination is represented by the letter **n**.

When calculating the average main effect of a factor of A, the equation 2.6 is applied by using the effect of A at the low level of B, [a – (1)]/n, and the effect of A at the high level of B, [ab – b]/n. Applying the contrast, which was stated before.

$$E_{fa} = \overline{y_{A+}} - \overline{y_{A-}} = \frac{ab + a}{2^{k-1} \cdot n} - \frac{b + (1)}{2^{k-1} \cdot n} = \frac{1}{2^{k-1} \cdot n} \cdot [ab + a - b - (1)] = \frac{Cons_A}{2^{k-1} \cdot n} \tag{2.6}$$

The same principle is applied when calculating the average main effect of B:

$$E_{fb} = \frac{Cons_B}{2^{k-1} \cdot n} \tag{2.7}$$

The final effect present is the average interaction effect of A and B, which is represented by the difference between the effect of A at the high level of B and of A at the low level of B. It’s possible to invert the order of the calculation and obtain the same result, as the interaction works equally both ways [38].

$$E_{fab} = \frac{Cons_{AB}}{2^{k-1} \cdot n} \tag{2.8}$$

By applying this to the example at hand,

$$E_{fa} = \frac{80 + 47 - 55 - 25}{2^{2-1} \cdot 1} = 23.5 \tag{2.9}$$

$$E_{fb} = \frac{80 + 55 - 47 - 25}{2^{2-1} \cdot 1} = 31.5 \tag{2.10}$$

$$E_{fab} = \frac{80 + 15 - 47 - 55}{2^{2-1} \cdot 1} = -3.5 \tag{2.11}$$

The main effects are both positive, suggesting that increasing A or B from low to high level with increase the result, but, as shown in the third effect, the interaction is negative, as its increase will result in a decrease in the result. It also has much lower impact on the result and, depending on the conditions and requirements of the experiment, might be considered unimportant [38].

2.3.2 Regression Model Representation and Response Surface

The next step in the analysis is the design of a RMR, which is the most intuitive way of expressing the results of the factorial experiment and, even though there is also the possibility of using an effects or means model, this was the chosen way to approach the problem (equation 2.12). One of the main uses of the RMR is also its application on the honing of the modelling parameters, as it can be used to predict the approximate response when the coded variables are other than -1 and 1.

$$y_{a,b...p,q} = \beta_0 + \beta_a x_a + \beta_b x_b + \beta_{a,b} x_{a,b} + ... + \beta_{p,...,q} x_{p,...,q} + \epsilon \tag{2.12}$$

Where the x_A and x_B are the coded variables which represent the levels of A and B (2.13), respectively, while the β's are the regression coefficients (also known as effects) and the ϵ is the residual (2.12). Applying the regression model to the example at hand (known as the fitted regression model) is done by calculating the average response of the experiment (β_0), and half of the calculated effect with equations 2.9, 2.10 and 2.11 for A, B, and AB for β_A, β_B, and β_{AB} respectively, as shown in equation 2.13. The regression coefficient is half of the effect estimates because they measure the effect of only one point change of the coded variables on the response (y) on a two-unit change (-1 to 1) [38].

$$y = 51.75 + \frac{23.5}{2} x_A + \frac{31.5}{2} x_B + \frac{-3.5}{2} x_{AB} + \epsilon \tag{2.13}$$

As shown in figure 2.9, the effect of the interaction between A and B is shown to have a relatively low impact on the results. But, depending on the problem at hand, there might be a need to account for more, or less, effects. The impact caused by the absence of

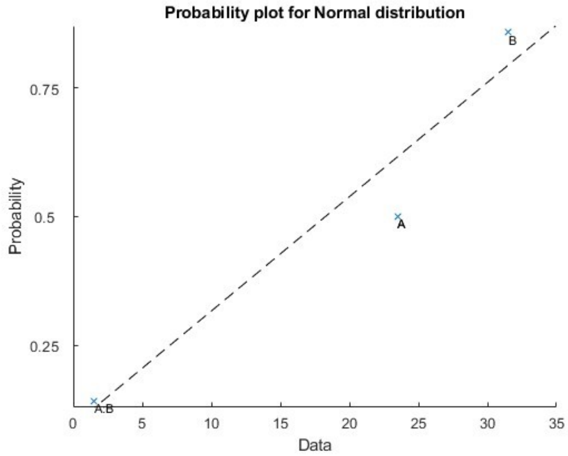

Figure 2.9: Normal probability plot (A, B and AB present the effects calculated in equations 2.9, 2.10 and 2.11

the interaction on the result was exemplified by adapting the regression model (equation 2.14).

$$y = 51.75 + \frac{23.5}{2} x_A + \frac{31.5}{2} x_B \tag{2.14}$$

When studying the residuals for A and B at high levels (ab), it's possible to show an example of the error of the approximation.

$$y = 51.75 + \frac{23.5}{2} \cdot 1 + \frac{31.5}{2} \cdot 1 = 79.25 \tag{2.15}$$

$$\epsilon_{ab} = 80 - 79.25 = 0.75 \tag{2.16}$$

While the value would be exact if the interaction was accounted for, the small error that results of it is, depending on the analysis, disposable. In this case, the error was of 0.938%.

The use of a RS (figure 2.10) is functional when a graphical representation of the regression model, which is the relationship between the combination of two, or more, variables and the outcome of the experiment is possible. In this case, the RS is close to flat because the effect of the interaction between A and B is close to zero.

2.3.3 Adjustment of the model

After obtaining the *regression model* and *response surface*, the next step in adjusting the values for each factor is, by making use of the *regression model*, to find the combination of factors that create the closest approximation to the objective.

With the *regression model* being a two-variable equation without the possibility of a system of equations, the chosen way to obtain the desired combination is by making use of the Monte Carlo method. By uniformly generating random numbers within [-1,1] for

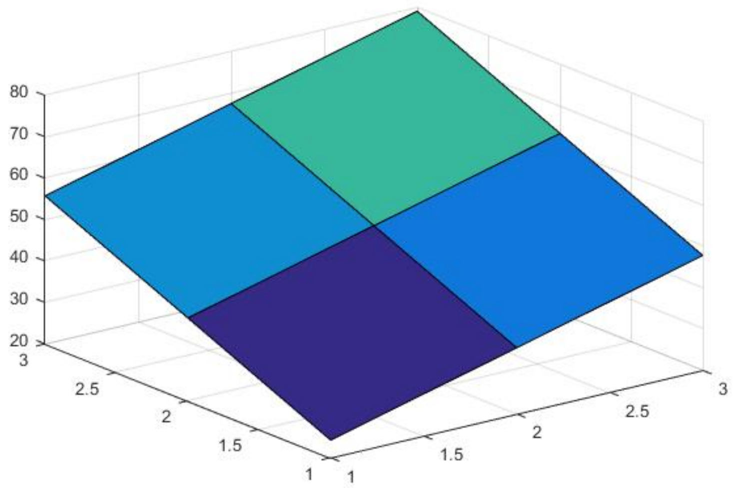

Figure 2.10: Response Surface

each factor and making use of the law of large numbers (by generating, in this case, a value $1 \cdot 10^5$ times for each variable), a lot combinations can be analyzed and, although the ideal one is not expected to be obtained, it can be closely approximated [38]. This process is done by using a computational algorithm available in *Matlab* software known as *rand*.

After running the method a minimum of five of times, the results converged to (table 2.4:

Table 2.4: Combinations with the lowest error. *Only applicable to the model that accounts all effects

	Factors		
Test number	A	B	AB*
1	0.535	0.474	0.279
2	0.406	0.452	-0.778
3	0.385	0.636	0.733
4	0.451	0.440	-0.584
5	0.641	0.307	-0.498
Average	0.451	0.452	-0.498

With an average absolute error of $5.05 \cdot 10^{-4}\%$ for each combination in each test when accounting for all effects, these results are good enough, but, due to the simple nature of the problem and low number of effects, it is visible in the table 2.4 that, even though the values do converge, the combinations tend to vary, most noticeably in the second order (the interaction between A and B, with a relatively high variance of 0.416), caused by the low effect of that the interaction has. This could be solved by increasing the amount of tests and combinations, but, due the amount of computational cost that would take, it is not justified in this exemplary problem. Although there are these limitations, the results will still be good enough to complete the objective of the example, as when applying the average value of the factors to equation 2.13, the result is 65.03, presenting an error of 0.046%, which is acceptable in this case.

The high variance presented in the interaction of second order also shows that, even when the value does change dramatically, the final result has a small change. This can be proved by the fact that the main effects of A and B only have an average variance of 0.012. Thus, when using the equation 2.14, the final result is 64.16 (equation 2.17), with an error of -1.29%. Although the error increases a lot, the error of only the significant effects is only 1.24% higher than its counterpart.

$$65 = 51.75 + \frac{23.5}{2} x_A + \frac{31.5}{2} x_B \rightarrow 51.75 + \frac{23.5}{2} \cdot 0,428 + \frac{31.5}{2} \cdot 0,463 = 64.07 \tag{2.17}$$

The values, even though randomly generated for each factor, need to be confirmed as independent in order to guarantee that all the combinations are legitimate and don't influence each other in their generation, as well as combination. So, the method used to analyze this is by applying the covariance in these two variables (equation 2.18) [38].

$$cov(A, B) = \mathbb{E}[(A - \mu_A) - (B - \mu_A)] \tag{2.18}$$

With μ being the expected values for A and B variables and $\mathbb{E}$ the expected value (also known as average) of, in this case, the covariance. In order to guarantee that the results are valid, as in each variable (x_A and x_B) is independent (or as close to it as possible), the covariance needs to be calculated as well, with an average result of $6.22 \cdot 10^{-4}$, $-9.3 \cdot 10^{-4}$ and $8.19 \cdot 10^{-4}$ for the relation of A-B, A-AB and B-AB respectively, it's safe to assume that the results are valid.

2.4 Experimental study

This section was based off of the studies made by the Department of Railway Structures of the Civil Engineering Faculty of the Czech Technical University in Prague [16] and by the Department of Civil and Environmental Engineering, Indian Institute of Technology in Patna, India [6]. These two studies apply themselves directly into the themes existing in this dissertation. Based on the nature of the current dissertation, the experimental study developed [16] is an experimental development and analysis of the response of a railway when under a cyclical load. The testing utilized as point of comparison for the current numerical model had the conditions presented in table 2.5. The laboratory measurement studied for this dissertation was the short-term Static analysis - slow loading of 50 cycles with an equivalent of 22.5t/axle.

Due to the conditions in which the tests were run, namely the physical properties of the brick clay, the permanent settlement presents higher values when compared to the numerical model, as the material that composes the brick clay is softer than the one

Table 2.5: Experimental measurement parameters [16].

	Material	Grain size [mm]	Depth [mm]
Ballast	Crushed aggregate (amphibolite)	32 to 63	0 to 35
Sub-grade	Crushed stone mixture	0 to 32	350 to 550
	Dry silica sand	0.3 to 0.8	550 to 570
	Rubber plates	-	570 to 662

present in a modern European railway. Thus, the permanent settlement and hardening (the difference between the last peak and the first) values obtained in such a study are not entirely similar when comparing to the numerical model, as it tends to be higher in absolute value. But the values obtained are still highly applicable and worth comparing. After 50 cycles, without the application of a geogrid, the average amplitude measured in the experiment was 0.753 mm (figure 2.11).

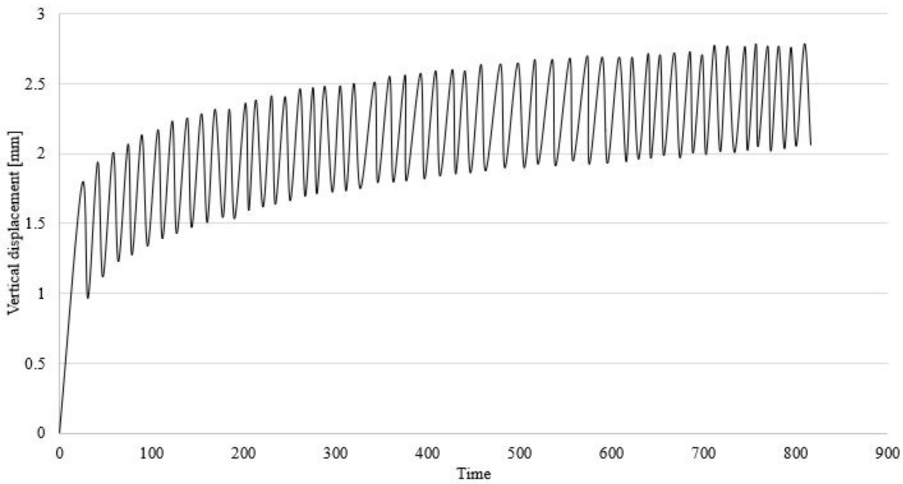

Figure 2.11: Graphical representation of the behaviour of the railway along 50 cycles (each peak representing a cycle) [16].

As for the influence of a geosynthetic (geogrid), the overall decrease in settlement is expected to be between 30% and 45% after 500000 cycles at 20Hz with 22.5t/axle [6, 16]. The use of a geogrid has a crucial impact when it comes to slowing down the detriment and, consequently, the settlement of the railway. This is justified by the increase in the bearing capability [16, 39] which is important because, with the increase in bearing ability, there is significantly less grain breakage (Ballast Breakage Index) which, in turn, decreases ballast and sub-ballast erosion, resulting in less settlement and longer longevity.

Although there is a significant increase in the overall performance of the railway when it's added a geogrid, the change in lateral behaviour (due to soil compactness) is only shown to be in the sections in contact (or in proximity) with the geogrid, presenting an increase in density and a decrease in the increment of consolidation in that direction, showing 31.81% less lateral deformation close to the geogrid [6]. As for a change in the mechanical properties (Young modulus, yield tension and tangent modulus), there are no clear signs that compaction and density in the ballast and sub-ballast have a linear or direct impact in these - showing the Friction angle and the contact area between the rocks to be better measuring parameters for ballast performance - as increased consolidation might mean the fouling of the rocks which constitute both sections of the railway [40], thus, further studies in this regard need to be developed.

3

Numerical Model

3.1 Introduction

In the development of the numerical model, there was interest in basing the structure in previous studies [33, 39] because of their approximations to the experimental models presented when under the same conditions. Several Static analysis were run in order to approximate the conditions of the experimental study, with low frequency ($6.15 \cdot 10^{-2}$ Hz with fictitious time) and 50 cycles for the initial definition, similar to the experimental study.

3.2 Design of the numerical model

The numerical model developed was, as stated, based in previous studies, with modifications made in order to improve it. Thus, this section shall - although the construction of the model is explained - focus on the tests and adjustments made in order to obtain the final model in the dissertation.

3.2.1 Geometry

When designing the model, its size is of the upmost importance, as the resolution regarding the resolution of the elements of the model has direct impact on the computational cost associated with the study. So, the size of the elements - length, thickness and width - need to be the biggest possible while guaranteeing good approximations (table 3.1) [33].

Table 3.1: General dimensions of the numerical model [33].

	Thickness [m]	**Width [m]**	**Spacing [m]**
Foundation	3	8	N/A
sub-ballast	0.3	5.2 (lower)	N/A
Ballast	0.3	4 (top)	N/A
Sleepers	0.22	2.6	0.6

With the cross section of the sleepers assumed to be a vertically symmetrical trapezium and having a top and bottom cross section width of 0.22 and 0.3m, respectively.

For simplicity, it was assumed that the loads applied on each rail are equal, so it's possible to create boundary conditions which emulate a symmetric structure along the vertical plane parallel to the rails (xy-plane), as shown in figure 3.1. This also helps reduce the computational cost [39].

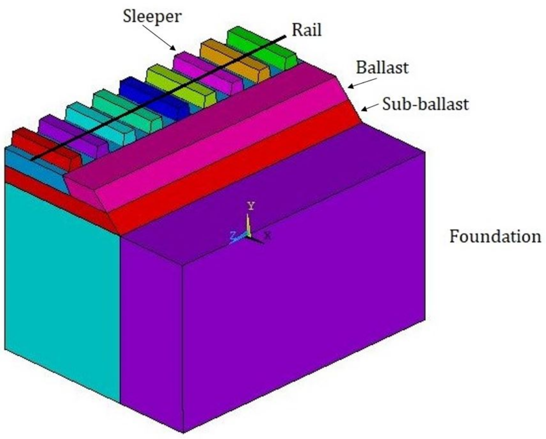

Figure 3.1: Overall railway sections.

When designing the mesh, a free mesh, although possible, is not the best approach for the problem, as its complexity and size imply a need for a well thought out process of meshing. Firstly, when meshing a model with different sections, as this one, the nodes created will share positions in the frontier between sections, as they belong to both volumes. Thus, to create a smooth transition, while also emulating the behaviour of these two sections, merging the nodes is the best option, since it creates nodes with the attributes of both layers (figure 3.2). This approach implies the need for the element size to be equal in transition areas in order to guarantee the presence of a contact surface between elements, which is also another reason to disqualify the use of free mesh [33].

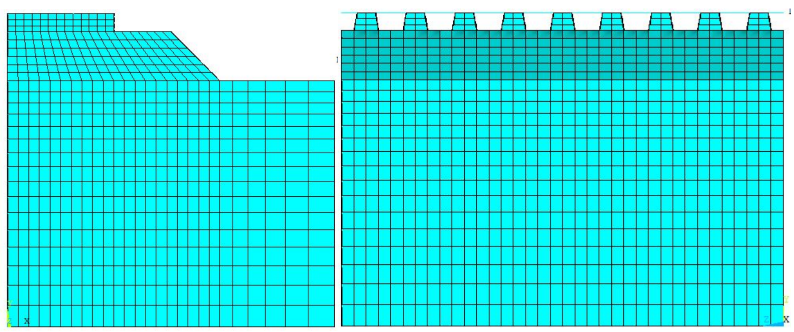

(a) Cross section mesh (b) Front representation

Figure 3.2: Mesh of the numerical model.

When analysing the model, the point of analysis has to be chosen based on the geometry of the overall structure, as well as the response that ensues when the load is applied (figure 3.3). A point over the rail is chosen because - although the computational cost is also significantly reduced - the study is primarily focused on the response and behaviour of the soil (that being the ballast, sub-ballast and foundation) and, by applying the load in a node of the rail that is in contact with the sleeper, the role of the rail in enduring a load is diminished, therefore, the vertical displacement obtained is close to uniquely the soils reaction and not the deformation of the rail. This choice of node also diminished the effect of the rail in the behaviour of the sleepers closest to the load if the load was applied between two sleepers, which would create a reaction in a direction contrary to that of the load.

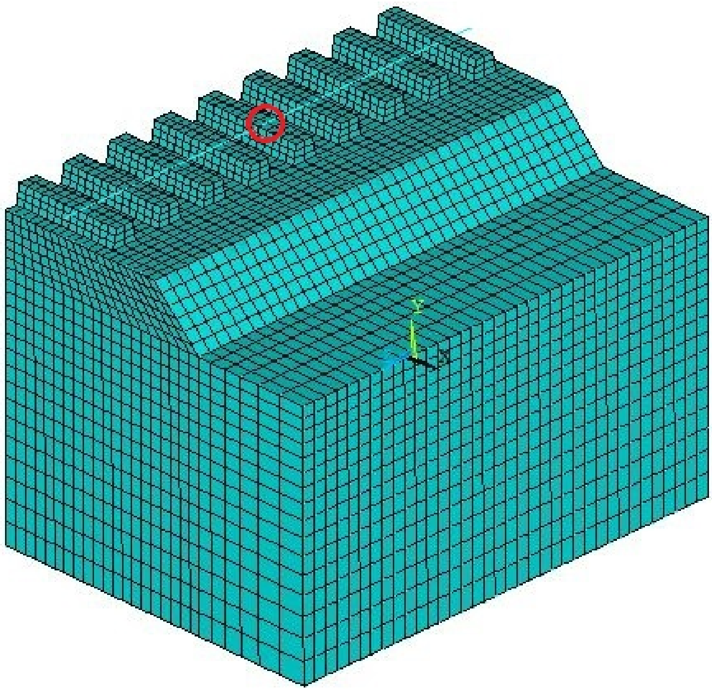

Figure 3.3: Node in which the load is applied.

3.2.2 Foundation and Sub-ballast

The foundation and sub-ballast have a relevant role when it comes to the long term development of the railway structure, with the foundation being the soil that, beneath the sub-ballast, supports all of the components of the track. With some railway tracks being long enough to cover entire continents, the physical properties of the soil tend to change a lot when there are severe geographical changes, so, all of the railway has to be built in order to maintain a strong and reliable structure throughout its the entire length.

As for the sub-ballast, it is the layer between the ballast and the foundation. The sub-ballasts main role is to prevent, not only contamination of the ballast by the foundation, but also to avoid the wear in the foundation caused by the loads applied and to allow for a good drainage of the railway. Hence, the sub-ballast tends to be composed of smaller sized components, when compared to the ballast. Thus, when it comes to developing a numerical model of the sub-ballast, there had to be added different physical properties than the ones applied on the ballast and foundation in order to emulate the numerical railway previously developed [16].

Even though the characteristics required by these two sections are indeed different, its safe to design them with SOLID185, as the versatility of the element type is enough to cover those distinctions, since, for example, water drainage is not accounted for in this model [35].

3.2.3 Geogrid and Ballast

As stated before in the sub-chapter 1.2.2.1, the main role of the geogrid is to reinforce and provide extra stability to the railway, to increase it's longevity and lower the investments made on maintenance. Being usually composed of polymer materials, it's physical parameters can have a wide range of values, but the ones used are presented in the table 3.2.

Table 3.2: Values of each parameter for the sleepers [33]

Young modulus [GPa]	**Poisson's Ratio**	**Density [kg/m^3]**
130	0.3	80

Being the geogrid a layer added between the ballast and sub-ballast and having a thickness relatively quite small when compared to the layers above and beneath, it is modelled with SHELL181 [37]. Then, the shared nodes are merged, creating a layer of nodes (and elements) where the proprieties are influenced by the geogrid, thus influencing the behaviour of the structure.

As for the ballast, it being the most notably relevant part of the structure in this project (due to its proximity to the rail and loads), with its main functions including, but not limited to: sleeper support, load bearing and transfer, vibration absorption and water drainage. Its properties had to be adjusted in order to achieve close proximity to the experimental tests made by [16]. The ballast is also the component where wear and tear tend to be the most notable and costly, which creates a higher need for resources and maintenance.

Thus, for the numerical model, the material chosen for the ballast is SOLID185, as it is used to model solid structures [35].

3.2.4 Sleepers, Railway fastening and Rail

The sleepers main purpose is spreading the loads applied along the ballast, supporting the fastening system and preventing lateral and longitudinal movement of the rails. Usually composed of reinforced concrete, due to the amount, and intensity, of the loads they withstand. An important variable in the application of sleepers is the spacing between each one, as the track behaviour is heavily influenced by it.

Table 3.3: Values of each parameter for the sleepers, these values derived from the research made in [39]

Young modulus [GPa]	Poisson's Ratio	Density [kg/m^3]	Spacing [m]
38	0.2	2400	0.6

Therefore, the sleepers are designed using SOLID185 due to the fact that this SOLID element is very versatile and can simulate sleepers, as long as the properties and parameters (table 3.3) are well defined [35].

When it comes to the railway fastening system (which incorporates the rail pads) its main focus is, not only to connect the rail to the sleeper, but also to absorb the vibrations and impacts that it's subject to by the use of railway pads. The stiffness of the railway pad is highly important due to the effect it has on the transmission of vibrations, and loads, to the structure below. So, due to the relevance of these parameters, whose relevance is mentioned previously (chapter 1.2.1.1), the parameters need to be well defined, as shown in table 3.4.

Table 3.4: Values of each parameter for the rail pads, values based on the research made in [39]

Young modulus [GPa]	Poisson's Ratio	Lateral to vertical stiffness ratio
1700	0.2	0.076

As the nodes that connect the rail and the sleeper are merged, the fastening of the system does not need to be added, as they are already connected. So, the only simulated component of the rail fastening system is the rail pad, which was created with COMBIN14, for its specialization in elasticity and damping (spring-damper) [36].

Thirdly, when developing the rail, which are made of hot rolled steel, BEAM188 is used. This is justified by, when cross section deformation is significant, the Timoshenko beam theory has to be used in order to correctly simulate the deformation with the use of the shear correction factor. The use of large deflection (accounting for changes in stiffness due to changes in the shape of the modelled volumes), in this case, is also crucial to a realistic simulation [34]. As for the European norms, there are two most widely used rail profiles are the vignole 54E1 and 60E1 (figure 3.4). The profile used is the 60E1, as it is the most widely used due to the fact that it connects to concrete sleepers (which are the ones being modelled).

3.2.5 Boundary Conditions

The boundary conditions were defined based on the results presented in previous studies [36], with the intent of simulating an extension of the model without having to design it, as a larger model (in terms of volume) would require a notably higher computational cost.

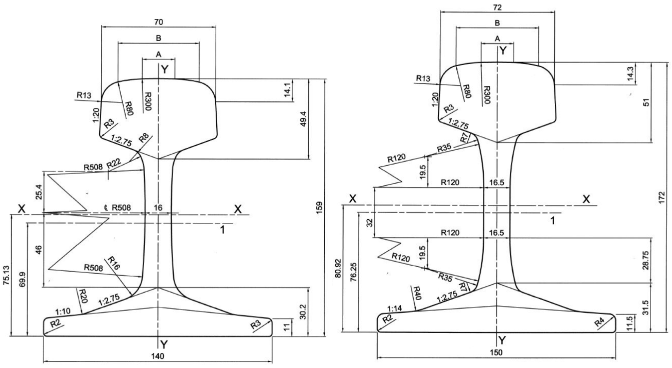

(a) 54E1 cross section (b) 60E1 cross section

Figure 3.4: Vignoles rail cross section [41].

3.2.5.1 Spring Constant

One of the major changes added to the previous model was the application of boundary conditions in the rails, which didn't exist before. In order to define the elastic conditions, it was necessary to create a relation between the Young modulus (E) and the spring constant K, in favour of the parameters available, those being I (moment of inertia), length of rail between two sleepers L and the cross section area A (equations 3.1, 3.2). The methods applied for the calculating the spring constants were the following [42]:

$$\delta = \frac{FL}{AE} \tag{3.1}$$

Which relates to the force of the spring which, in this case, is representative of the transversal resistance to deformation of the rail (equation 3.2):

$$K = \frac{AE}{L} \tag{3.2}$$

with δ representing the physical deformation of the spring, ε meaning the strain and σ representing the tension.

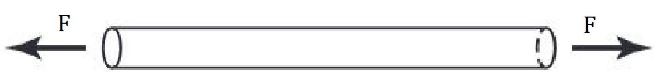

Figure 3.5: Simplified representation of a spring under longitudinal load [42].

The spring constant (K) was only applied in the vertical direction, with a simplified representation in the figure 3.5, as well as the moment around the X axis (figure 3.6), as the structure is only subject to vertical loads, which is not the case with the damping, that is applied in all three axils.

As for the rotational spring constant around the X axis, the method of obtaining said constant differs due to the fact that the motion of the spring is rotational, as presented in the following equations (3.3, 3.4):

$$\zeta = \frac{FL^3}{3EI} \tag{3.3}$$

with ζ representing the physical deformation of a rotational spring.

Applying the same reasoning as in the previous equations (3.1 and 3.2, the rotational spring constant is obtained with (equation 3.4)):

$$K = \frac{3EI}{L^3} \tag{3.4}$$

Figure 3.6: Simplified representation of a spring under rotational stress [42].

After the spring constant was determined (table 3.5), the next step was to obtain the damping ratio relative to the rail, as well.

Table 3.5: Values relative to the spring constant, transversal and rotational.

	Transversal modulus [GN/m]	**Rotational modulus [MN/rad]**
Spring modulus	9.37	4.00

3.2.5.2 Damping Ratio

The X and Y axis (horizontal and vertical axis, respectively) are calculated in similar fashion, as the waves that propagate in both directions are of shearing nature, contrary to the ones in the Z axis, which interact with the structure in the form of pressure (mostly known as longitudinal waves) due to the different axis of analysis [39]

For the X and Y axis, the shear modulus (G) of the rail is obtained by applying 3.5.

$$G = \frac{E}{2(1+\nu)} \tag{3.5}$$

In 3.5, ν is representative of the Poisson ratio.

The shear modulus is then related to the propagation of shear waves through 3.6.

$$CSR = \sqrt{\frac{G}{\rho}} \tag{3.6}$$

with ρ referring to the density of the rails.

Finally, the shear damping ratio is obtained with 3.7

$$CRT = \rho \cdot CSR \cdot A \tag{3.7}$$

As for the longitudinal wave propagation (Z axis), the material and ground properties react differently when compared to shear deformation, subsequently creating the need for a different approach when it comes to the damping ratio.

For the Z axis the method of calculus is similar. The oedometric modulus, MOed (equation 3.8) is applied, as it applies to the compressing deformation to a laterally confined material, thus obtaining the MOed:

$$Moed = \frac{E(1-\nu)}{(1+\nu)(1-2\nu)} \tag{3.8}$$

After obtaining the MOed (equation 3.8), the relation referencing the propagation of longitudinal waves is shown in 3.9.

$$CPR = \sqrt{\frac{Moed}{\rho}} \tag{3.9}$$

Subsequently, the longitudinal damping ratio derives from 3.9 through the following equation 3.10:

$$CRM = \rho \cdot CPR \cdot A \tag{3.10}$$

After attaining the values relative to the damping (table 3.6), it's clear that it has a significant impact when it comes to the settlement recorded with the developed numerical model because, by restricting freedom of movement of the railway track, the work of the load will also be focused in the damping. Also, by simulating the continuation the rail, the simulation will be more accurate.

Table 3.6: Values relative to the damping coefficient, transversal and rotational.

	Transversal damping [kNs/m]	**Longitudinal damping [kNs/m]**
Damping coef.	193.13	36.13

3.3 Physical Properties

With the shape and divisions of the model already defined, as well as the boundary conditions, the physical properties need to be defined in order to accurately emulate the experimental model [16] to which the results are being measured against. In this phase, a rough approximation to the behaviour of the experimental model is done, in order to create the basis for an in depth study of, not only the best combination of physical properties, but also the influence and role each property plays in the overall behaviour of the railway.

The Static analysis were run in accordance to the frequency used in the physical model [16], creating similar conditions in both cases. The parameters used for comparison were the final settlement, average amplitude after 50 cycles, hardening and first peak.

3.3.1 Study of parameters

At first, a simulation with the average values of each section was run (table 3.7), at which the deviation was then calculated against the experimental model (table 3.8), thus giving an estimate of how, not only the numerical, but also the experimental model, differ from the average.

Table 3.7: Average physical properties from each section of the model [39].

	Foundation	**Sub-ballast**	**Ballast**
Young modulus [MPa]	100	129	170
Yield tension [kPa]	N/A	16.550	15.550
Tangent modulus [kPa]	N/A	239.975	225.475

With the hardening effect being defined as the difference between the first and last peak, the amplitude being the amplitude of the harmonic behaviour, the settlement as the last lower peak and the first peak as the first peak that the structure achieves in the first load application, when run with the values presented at the table 3.7, the average absolute deviation was too high to be useful in the study (table 3.8), as a result, further testing, with different initial parameters, needed to be run.

Table 3.8: Average parameters results compared to experimental results [16].

	Experimental	**Simulation**	**Deviation [%]**
Amplitude [mm]	0.753	0.852	-13.15
Settlement [mm]	2.061	1.686	18.19
First peak [mm]	1.781	2.044	-14.77
Hardening [mm]	1.002	0.454	54.69

After the results presented in table 3.8 and in figure 3.7, it's clear that a change in the parameters is needed in order for the Design of Experiments to be applicable, so, after analysing the simulation, the first peak and amplitude are too high, while the settlement is too low. This presents a need for an increase in the Young modulus for both the ballast and sub-ballast, as shown in the table 3.9 in order to approximate the first peak and the amplitude (which are two parameters that are almost exclusively "operate"within the elastic realm). The hardening is also severely different between the two, which also indicates a need for adjustments.

With the present parameters, although the deviation is still high to be considered a good standard to further develop the project as is, it does have an average absolute deviation closer to 10%, with the amplitude being close to 8% (table 3.10), which was,

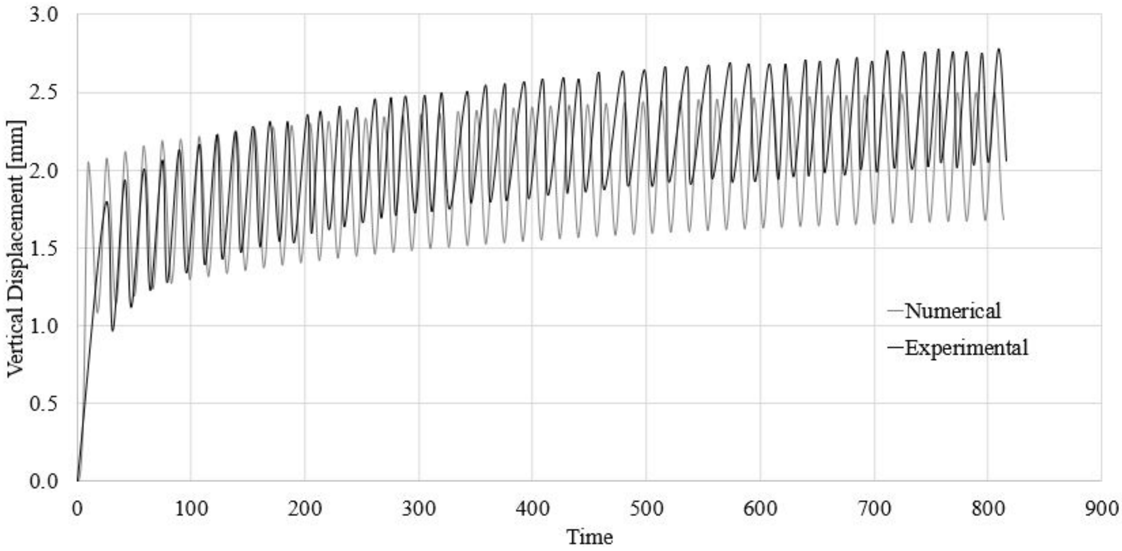

Figure 3.7: Graphical comparison between the numerical and experimental results.

Table 3.9: Adjusted physical properties for each section of the model.

	Foundation	**Sub-ballast**	**Ballast**
Young modulus [MPa]	100	170	210
Yield tension [kPa]	N/A	16.550	15.550
Tangent modulus [kPa]	N/A	239.975	225.475

as shown, not the case before. With these approximations, the 2^k factorial has a better chance at approximating the values and creating a closer approximation.

Table 3.10: Results for adjusted parameters compared to experimental results.

	Experimental	**Simulation**	**Deviation [%]**
Amplitude [mm]	0.753	0.817	-8.49
Settlement [mm]	2.061	1.739	15.62
First peak [mm]	1.781	2.013	-13.03
Hardening [mm]	1.002	0.462	53.89

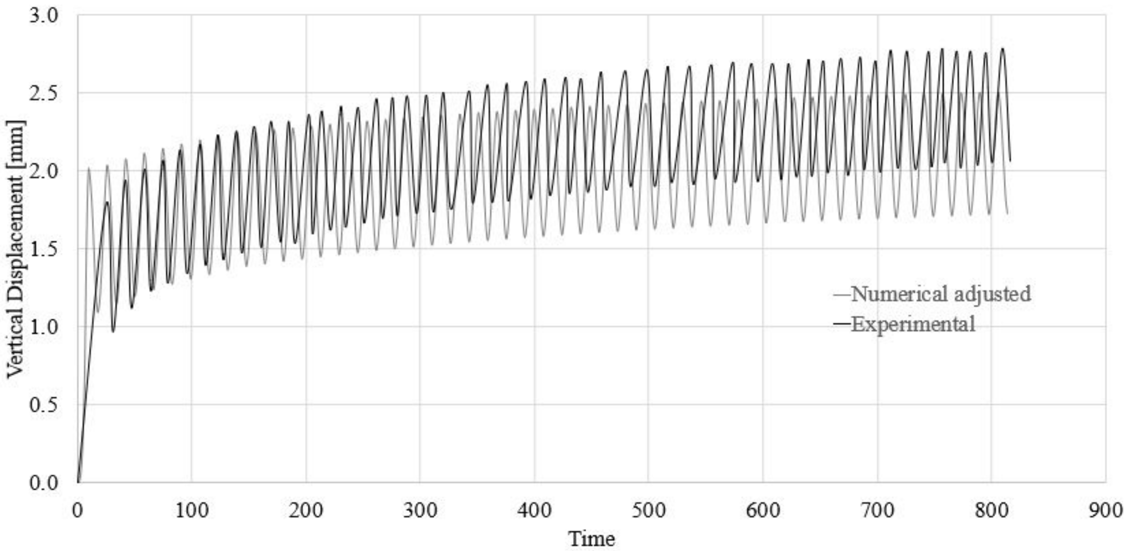

Figure 3.8: Graphical comparison between the (adjusted) numerical and experimental results.

4

Results and Discussion

4.1 Introduction

With the initial parameters defined, it is possible to start studying the model on a deeper level. Thus the base values for the parameters were changed and tested in this new phase (table 4.1)

To make an organized study, a design of experiments is used in order to analyse accurately how changes in the parameters, and combinations, lead to different results in the simulations made. The aim of a full factorial analysis in this case is the examination of the role and amount of influence each parameter has in the behaviour of the model, as well as to find the ideal combinations for the model so as to make it as realistic as possible. Then, by honing the parameters of the model, a final combination is obtained.

4.2 Study of parameters

Applying variations of 15% (these variations were chosen so that it's possible to analyze the structure without increasing too much the values of the factors as, with higher changes, further studies would need to be done to confirm the values for the mechanical properties), each parameter has a change of either -15% or 15% in a 2^k factorial design. Tests are run in an effort to evaluate how each possible combination modifies the behaviour of the structure in the first peak, amplitude, settlement and hardening. In order to test every possible combination, a total of 64 (a 2^6 factorial study) simulations were run. Due to its assumed low influence compared to the other two sections, the foundation was not a part of the parameters studied in the first set of experiments, so, the parameters that are tested in this phase belong to the ballast and sub-ballast, those being the Young and tangent modulus as well as the yield tension, resulting in six parameters and 64 analysis.

4.2.1 First phase

The analysis of all 64 combinations showed that, although the settlement and first peak are not yet acceptable, it is of note that, in the simulation 37, with the parameters and

Table 4.1: Physical properties from each section of the model.
*Parameter not susceptible to change in the first phase.

	Foundation	Sub-ballast	Ballast
Young modulus [MPa]	100*	170	210
Yield tension [kPa]	N/A	15.550	16.550
Tangent modulus [kPa]	N/A	239.975	225.475

results shown in tables 4.2 and 4.3, respectively, there is a close resemblance in the overall behaviour of the structure (shown in the figure 4.1 by the close rate of settlement and hardening in both analysis). This shows that, with further adjustments to the values of the mechanical properties, it's possible to create a more realistic approximation. It's also important to note that the amplitude has an error of -9.29%, showing resemblance in this particular model.

Table 4.2: Physical properties for the model 37 for each section.

	Foundation	Sub-ballast	Ballast
Young modulus [MPa]	100	195.5	241.5
Yield tension [kPa]	N/A	14.068	13.218
Tangent modulus [kPa]	N/A	203.979	191.654

Table 4.3: Results for the model 37 compared to experimental results.

	Experimental	Simulation	Error [%]
Amplitde [mm]	0.753	0.823	9.29
Settlement [mm]	2.061	2.679	29.99
First peak [mm]	1.781	2.599	45.93
Hardening [mm]	1.002	0.871	-13.07

As shown, although the settlement and first peak are still quite far from what is considered optimal, the global hardening and amplitude are very closely approximated, thus providing a basis for further development.

But, as referred previously (section 2.3), to check if all the parameters that are being tested have a significant effect on the results of the simulations, an effect analysis was made (Figures 4.2 and 4.3). In table 4.4, it's shown that each parameter has been appointed a letter for easier identification on each graph in the figures 4.2 and 4.3).

The letter F, which is appointed to the sub-ballast's tangent modulus, is shown to be over the vertical line present in the data point of zero in three of the four graphs (figure 4.2 and 4.3). This implies that the F factor has a negligible influence over the behaviour of the model, thus, having it as a variable in the 2^k factorial is not a practical choice, being a waste of computational cost. So, in the next phase, the foundation's Young modulus takes the place of the sub-ballast's tangent modulus as the sixth factor. Another significant take

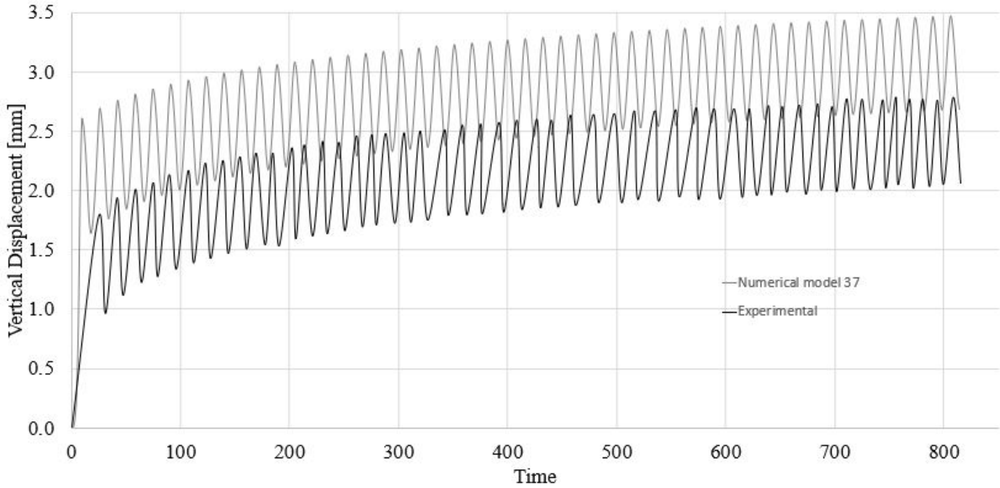

Figure 4.1: Graphical comparison between the model 37 and experimental results.

Table 4.4: Appointment of letters to each parameter.

	Variable	Factor
Ballast	Young modulus	A
	Yield tension	B
	Tangent modulus	C
Sub-ballast	Young modulus	D
	Yield tensions	E
	Tangent modulus	F

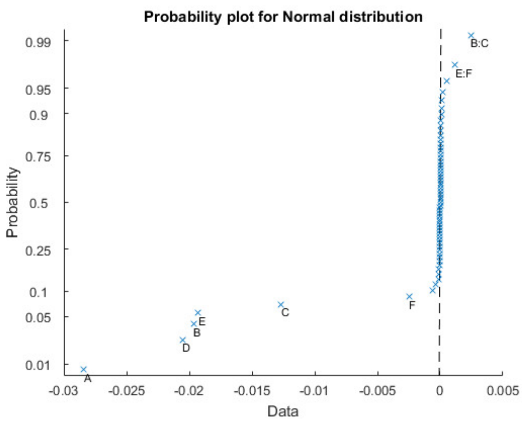

(a) Amplitude

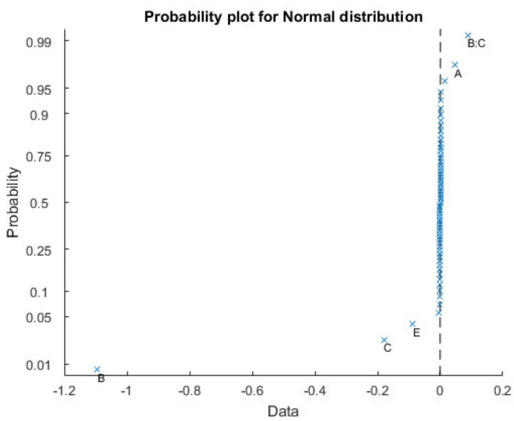

(b) Settlement

Figure 4.2: Graphical representation of effects in probability plots for the amplitude and settlement.

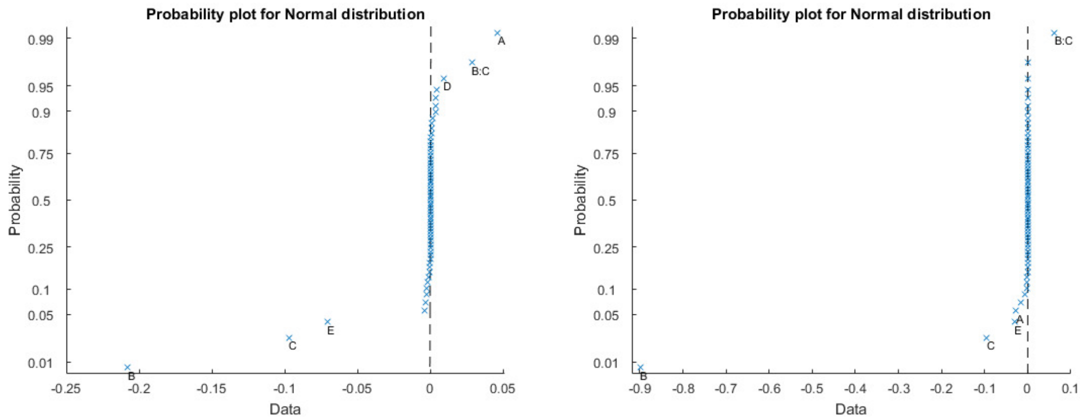

(a) Hardening (b) First peak

Figure 4.3: Graphical representation of effects in probability plots for the global hardening and first peak.

from the influence analysis is the amount of influence that the factors A and B have within the model, this was expected, as the ballast is the most significant part of the structure in this model and when performing these types of studies - which justifies the reason why so much effort is put into the making of ballasts in experimental studies, as shown in the experimental tests used as reference in this dissertation [6, 16].

4.2.2 Second phase

After the results of the first phase, in which the model 37 was picked as the most similar in overall behaviour, a second Design of Experiments was run in order to demonstrate the viability of the previous Design of Experiments and to design the RMR, this time with the set of parameters which compose the model 37 as base values (table 4.2). In this new set of simulations, the foundations Young modulus is the sixth parameter (F) in the 2^6 factorial design. The change executed in each parameter remains the same as before, that being 15% and the number of simulations is also 64, the same as previously, table 4.5.

Table 4.5: Appointment of letters to each parameter.

	Variable	**Factor**
Ballast	Young modulus	A
	Yield tension	B
	Tangent modulus	C
Sub-ballast	Young modulus	D
	Yield tensions	E
Foundation	Young modulus	F

After the simulations were completed, the model which resembles the study of L. Horníček and Tyc [16] study the most is number 18. With the results presented in the table 4.6, it's shown that this model has an approximation satisfactory to the demands set in this phase, as presented, not only in the table 4.7 by the relatively low value of error, but also in the figure 4.4.

Table 4.6: Physical properties for the model 18 for each section.

	Foundation	Sub-ballast	Ballast
Young modulus [MPa]	115	166.175	205.275
Yield tension [MPa]	N/A	11.957	15.200
Tangent modulus [MPa]	N/A	203.979	162.906

Table 4.7: Results for the model 18 compared to experimental results.

	Experimental	Simulation	Error [%]
Amplitude [mm]	0.753	0.810	-7.59
Settlement [mm]	2.061	2.179	-5.70
First peak [mm]	1.781	2.139	-20.08
Hardening [mm]	1.002	0.805	19.62

With all experimental results (with the exception of the global hardening, which, although it doesn't fall into it, it's close to it) falling within the response surface, the model 18 provides further evidence that it is a viable basis for designing the RMR for the adjustments.

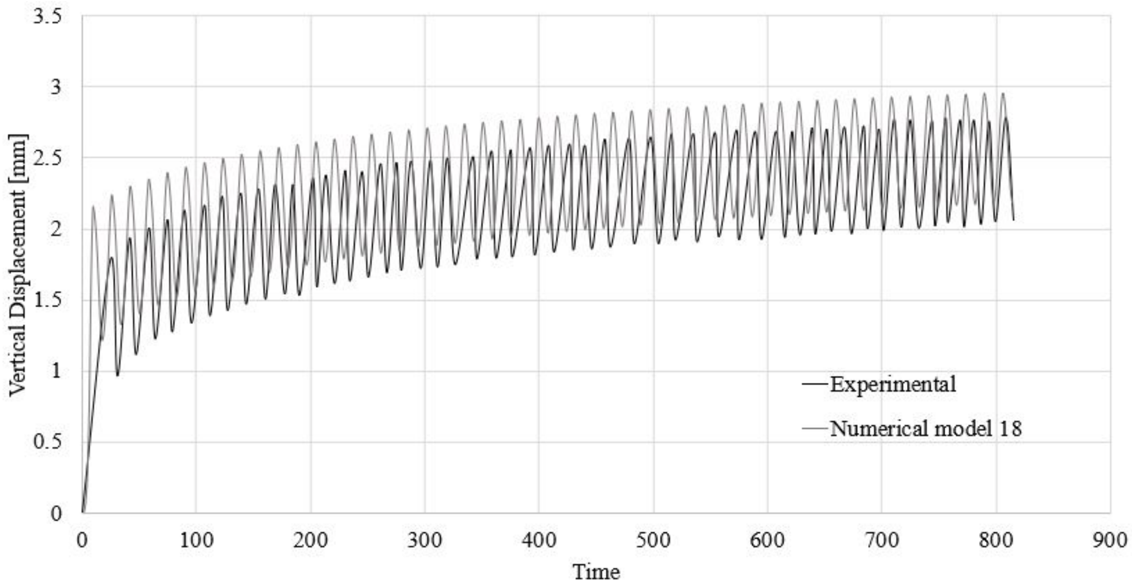

Figure 4.4: Graphical comparison between the model 18 and experimental results.

After the exchange between the tangent modulus of the sub-ballast and the foundation's Young modulus, every factor was relevant in at least one result. The figures 4.5 and 4.6 provide confirmation.

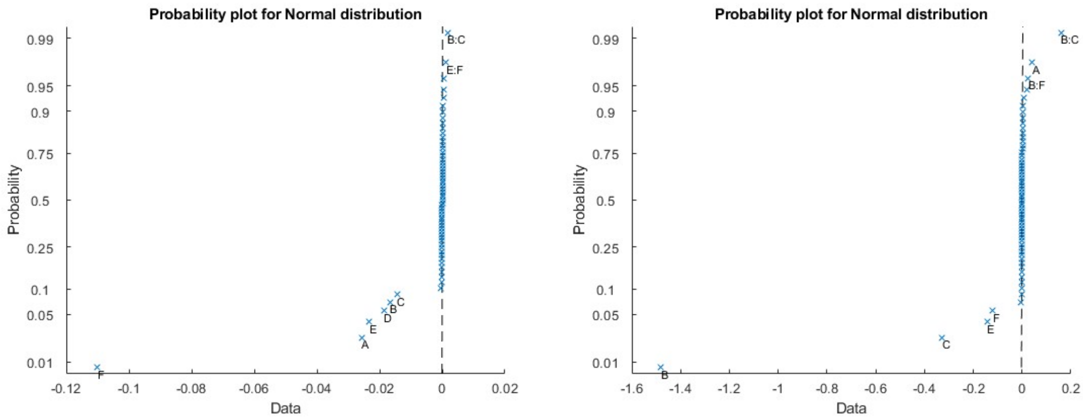

(a) Amplitude (b) Settlement

Figure 4.5: Graphical representation of effects in probability plots for the amplitude and settlement.

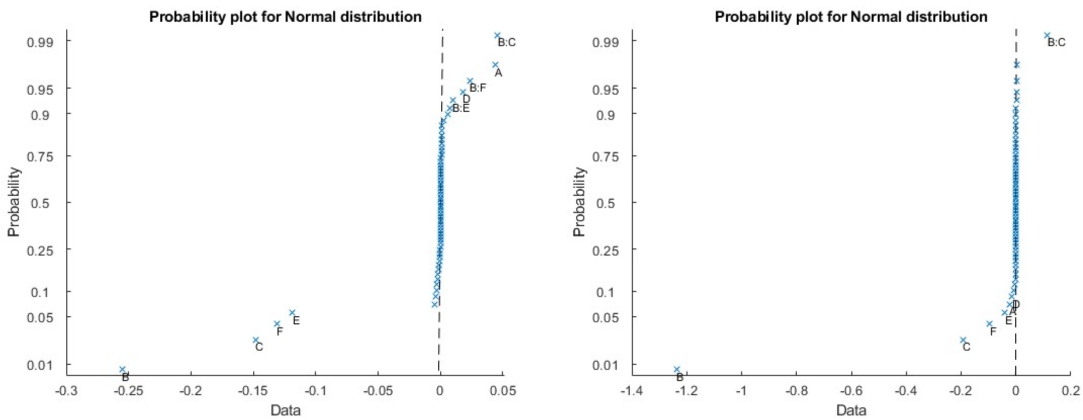

(a) Global hardening (b) First peak

Figure 4.6: Graphical representation of effects in probability plots for the global hardening and first peak.

After the study, the results shown fall within the interval of results which affirms that the development of the RMR is justified. For a second time, with the use of *Matlab* software, the effects were obtained for each parameter in study (table 4.8) and a RMR was developed for each criteria of evaluation (amplitude, settlement, global hardening and first peak) based on equation 2.12.

With these effects, it's possible to write the RMR for, for example, the first peak (equation 4.1):

$$y_{FP} = 2.734 + 0.0236x_A - 1.237x_B - 0.193x_C - 0.0406x_E - 0.0966x_F - 0.115x_{BC} \quad (4.1)$$

Thus, given the results obtained with these two cycles of testing, honing is the next,

Table 4.8: List and values of significant direct and interaction of effects per result.

	Factor	Effect
Amplitude	A	-0.0257
	B	-0.0167
	C	-0.0144
	D	-0.0187
	E	-0.0233
	F	-0.110
	BC	0.00174
	EF	0.00120
Settlement	A	0.0422
	B	-1.481
	C	-0.0327
	E	-0.143
	F	-0.120
	BC	0.160
	BF	0.0243
Global Hardening	A	0.0438
	B	-0.255
	C	-0.148
	D	0.0178
	E	-0.119
	F	-0.131
	BC	0.457
	BE	$9.722 \cdot 10^{-3}$
	BF	0.0234
First peak	A	-0.0236
	B	-1.237
	C	-0.193
	E	-0.0406
	F	-0.0966
	BC	0.115

and final, step in the development of the model, which is to find the values for each factor that better approximate the results of the RS to the experimental results.

4.2.3 Honing of the model

Due to the inability to analytically solve the system of equations, the Monte Carlo method was used. Thousands of simulations were made - based on the values presented in table 4.2 - where $1 \cdot 10^6$ random numbers were generated for each of the six factors within the interval [-1.5,1.5] (by increasing the interval, there is a better chance of finding a viable option for the equations), with each combination and result stored in a matrix, with the lump sum and euclidean norm of the errors for each result as well. Then, in order to obtain the best overall combinations, the lowest euclidean norm and lump sum of the percentage of errors relative to the experimental tests for each result were used as a means to select the best combinations. After gathering 16 of the best straight results (presented in appendix A), the factors converged to two combinations (tables 4.10 and 4.11).

Although there is convergence of values, with the Monte Carlo method being a statistical process, for each factor there is always variance. To be able to guarantee convergence and reliability of the results, the variance, as well as the covariance have to be analysed. So, as presented in tables 4.10 and 4.11, there are some factors which have a higher variance than others but these results are not much of a liability because those that tend to have a higher value of variance also tend to have the least influence in the results, therefore their average values are also reliable, in this case. As for the covariance, the first step is the analysis of the matrix representative of the relationship between each factor, so as to guarantee the independence of each variable. It is presented in table 4.9, with the values being the average of all the tests run in the process of this dissertation.

Table 4.9: Covariance matrix of the values generated by the Monte Carlo method.

Covariance	**A**	**B**	**C**	**D**	**E**	**F**
A	0.334	-0.003	-0.003	0.004	-0.005	-0.001
B	-0.003	0.763	-0.005	-0.006	0.010	-0.017
C	-0.003	-0.005	0.740	-0.002	0.003	0.012
D	0.004	-0.006	-0.002	0.754	-0.009	0.009
E	-0.005	0.010	0.003	-0.009	0.739	-0.003
F	-0.001	-0.017	-0.012	0.009	-0.003	0.738

As shown, the joint variability is very close to zero when measuring the variability of two different factors, providing certainty about the reliability of the results.

Table 4.10: Overall analysis of the first convergence. *All effects up until the second order

Variable	**Effects**	**Variance**	
A	1.471	$1.922 \cdot 10^{-3}$	
B	1.329	$6.624 \cdot 10^{-3}$	
C	-1.252	$2.103 \cdot 10^{-2}$	
D	1.323	$3.109 \cdot 10^{-1}$	
E	-1.321	$4.649 \cdot 10^{-2}$	
F	0.639	$1.495 \cdot 10^{-1}$	
	All effects*	**Significant effects**	
Lump sum	25.58	26.26	
Norm	15.89	16.24	
	Foundation	**Sub-ballast**	**Ballast**
Young modulus [MPa]	109.590	234.909	295.397
Yield tension [kPa]	N/A	11.306	15.831
Tangent modulus [kPa]	N/A	203.979	155.932

Table 4.11: Overall analysis of second convergence. *All effects up until the second order

Variable	Effects	Variance	
A	0.917	$5.989 \cdot 10^{-3}$	
B	1.359	$4.577 \cdot 10^{-3}$	
C	-1.438	$5.254 \cdot 10^{-2}$	
D	1.076	$2.565 \cdot 10^{-1}$	
E	-1.412	$6.608 \cdot 10^{-3}$	
F	0.621	$1.826 \cdot 10^{-1}$	
	All effects*	**Significant effects**	
Lump sum	27.64	28.51	
Norm	16.36	16.74	
	Foundation	**Sub-ballast**	**Ballast**
Young modulus [MPa]	109.314	227.629	275.269
Yield tension [kPa]	N/A	11.114	15.892
Tangent modulus [kPa]	N/A	203.979	150.594

As expected, when accounting for more effects, the results tend to be better, but it is also an opportunity to understand that, although there is a difference in results, they're not significant enough to need to be accounted for, as figures 4.5 and 4.6 present.

When comparing both convergences, the factor that had the largest change was A, which accounts for the E of the ballast, while the other factors have smaller changes. In the second convergence, the norm and lump sum are higher than in the first but there are reasons to still study the second convergence. Firstly, having increased the interval of values for each factor from [-1,1] to [-1.5,1.5], there is a decrease in the reliability of the RMR when predicting the FEM behaviour, as the RMR was designed for the smaller interval and there are no guarantees that the structure will have the same behaviour. Secondly, having a lower value for the Young modulus is a positive aspect, as having increasingly higher values for it will tend to make the values for the modulus of elasticity less realistic. Thus, simulations were run using both convergences and the results are presented in table 4.12.

After running both FEM simulations presented in figure 4.8 and 4.7, even though the results are quite similar and the figures don't show a difference. Tables 4.12 show that there are slightly better results when using the first convergence, but, after analysing the both convergences, and the average values for mechanical properties in European railways, the second convergence was chosen as the basis for the application of the geogrid. The difference in error, being roughly two decimals, is possible to overlook in order to guarantee values for the physical properties of both the ballast and sub-ballast that are closer to real world surveys [39].

Using the second set of parameters in FEM, the stress state ratio is calculated when the load is first applied on the model (figure 4.16(a)). As shown, plastic deformation exists almost exclusively in the ballast and sub-ballast, demonstrating how significant

Table 4.12: Results of FEM simulation.
*Error of the FEM simulation compared to the experimental results.

First Convergence			
Parameter	**Results with FEM [mm]**	**Results with RMR [mm]**	**Deviation* [%]**
Amplitude	0.774	0.777	-2.76
Settlement	2.164	2.020	-4.98
First peak	2.014	0.879	-13.09
Hardening	0.885	1.917	11.68
Average absolute error			8.13
Second Convergence			
Parameter	**Results with FEM [mm]**	**Results with RMR [mm]**	**Deviation* [%]**
Amplitude	0.786	0.777	-4.36
Settlement	2.157	2.025	-4.67
First peak	2.014	0.839	-13.10
Hardening	0.889	1.925	11.22
Average absolute error			8.34

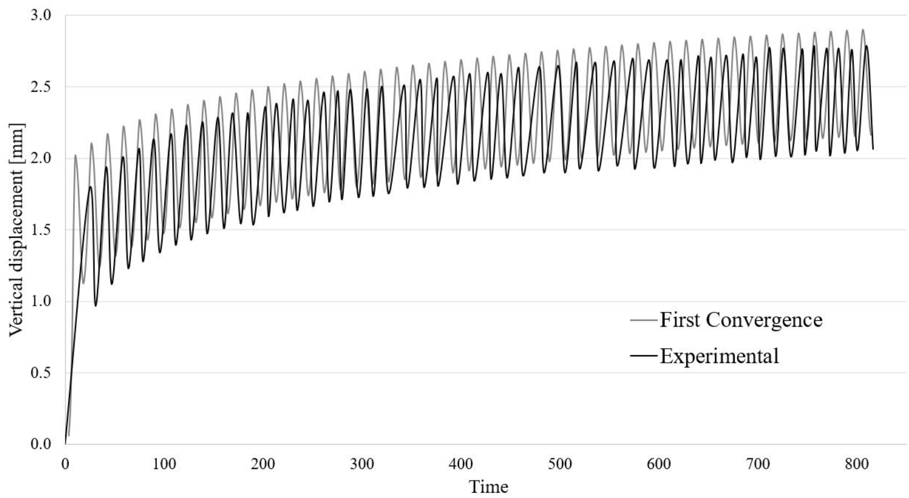

Figure 4.7: Numerical model behaviour with the first convergence parameters.

the roles of those two sections are in the model.

The deformation occurring in the model is represented in figure 4.10 with a magnification ratio of 170.

After the final adjustment phase, it's then possible to begin the study of the geogrid and how it affects the behaviour of the overall structure through the compaction of the layers in contact with it. As previously mentioned in chapter 2.4, due to the construction of the experimental model [16], it cannot be totally replicated with the current numerical model, but it can be closely approximated with similar behaviour.

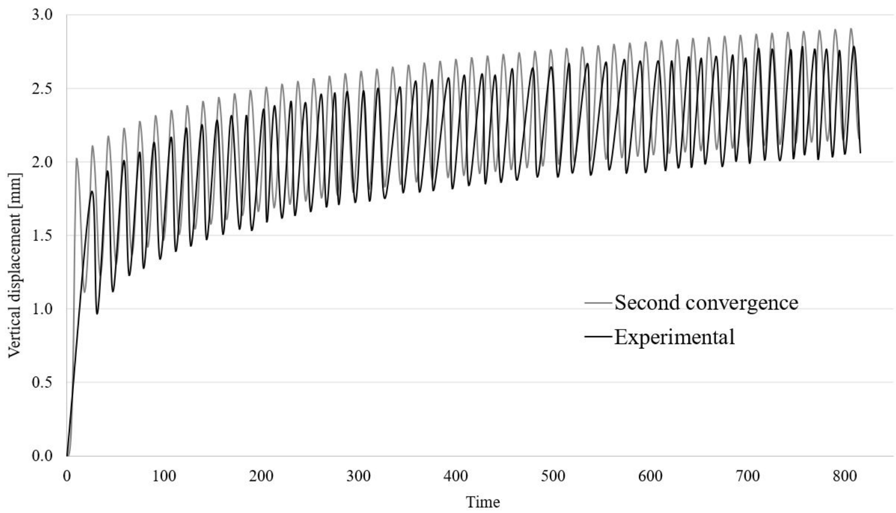

Figure 4.8: Numerical model behaviour with the second convergence parameters.

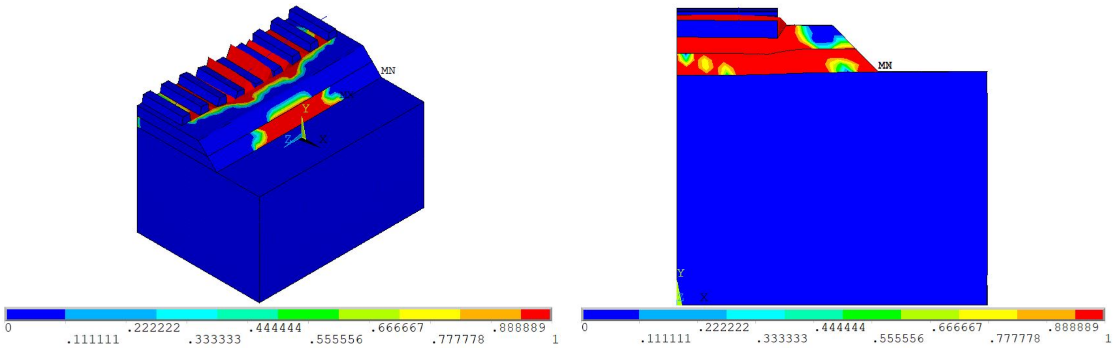

(a) Stress state ratio in isometric view

(b) Stress state ratio in section view

Figure 4.9: Overall distribution of stress within the model.

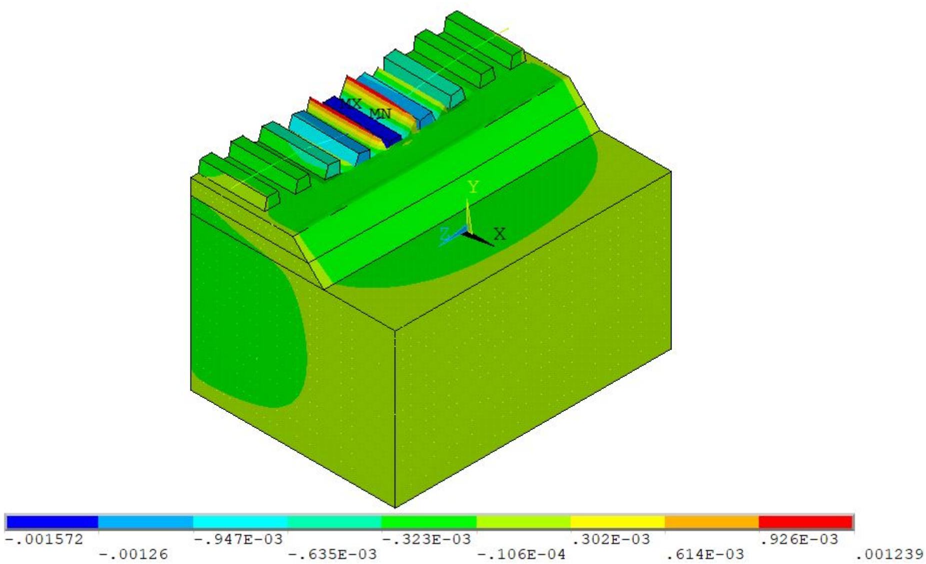

]Displacement field of the model with the first application of load [m].

Figure 4.10: .

4.3 Geogrid

After the model was developed, the start of the study of the presence of a geogrid was initiated. As referred in chapter 2.4, the major change in the behaviour of the structure occurs in the region of ballast and sub-ballast that are close to, or in contact with the geogrid. This is justified by the increased compaction and interlock that happens in those volumes of the ballast and sub-ballast, resulting in an increase of the Friction angle in those short sections. The geogrid was modelled by adding a SHELL181 element between the ballast and sub-ballast of the model.

To study the settlement of the railway, the first step was analysing the addition of a shell element in the position of the geogrid without accounting for compaction and comparing it to the settlement of the numerical model without the presence of a shell element (figure 4.11). By merging the nodes of the ballast and sub-ballast with those of the geogrid, that area becomes influenced by the geogrid and, in turn, influences the elements in to which the nodes belong to.

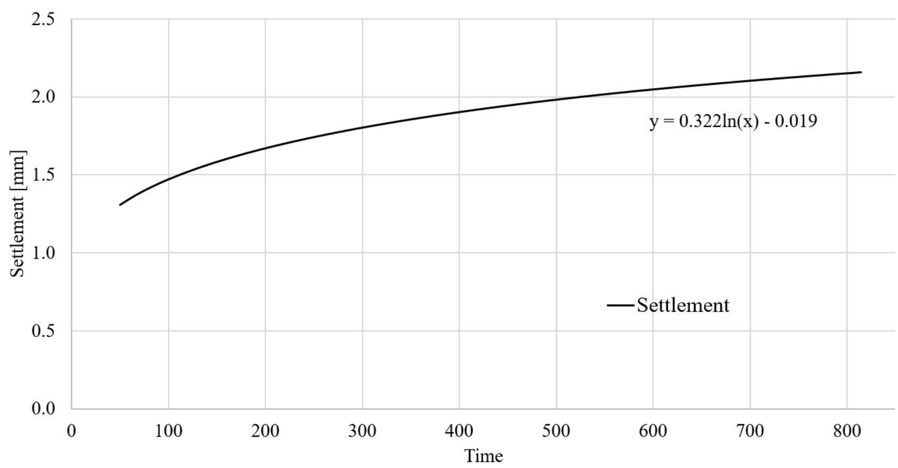

Figure 4.11: Evolution of the settlement along 50 cycles.

By making use of the logarithmic function, the overall behaviour can be approximated and used as a basis to approximate the evolution of the settlement. With the slope of the logarithmic function in figure 4.11 being 0.322, it's safe to assume that, with an improvement between 30 and 45% [6], the slope should be within 0.19 and 0.24.

4.3.1 Geogrid and no compaction

To understand how the addition of the shell element influences the behaviour of the model, a FEM simulation was run. This way, the starting point of the study is understood and the results gain better context when it comes to the influence of the shell element without compaction. In table 4.13 and figure 4.12 the results present a small change in the settlement of the model, but, those small changes were the lowering of the criteria of study, which also indicates improvement.

Table 4.13: Results and improvement of FEM simulation with geogrid without compaction compared to without geogrid.

Parameter	Result [mm]	Improvement [%]
Settlement	2.134	1.07

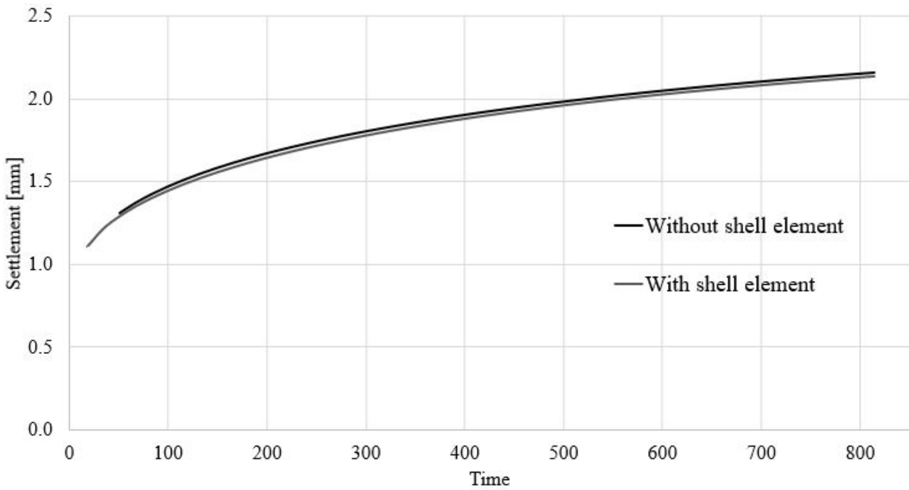

Figure 4.12: Numerical model behaviour with the presence of a geogrid compared to without it. Showing a small improvement.

With this result, the addition of a geogrid without the accounting for the compaction of the ballast and sub-ballast is not enough to reach significant improvement. But, with the improvement in the results, it is clear that the inclusion of a geogrid has a positive influence in the behaviour of the model, which is a positive indicator of the influence of the geogrid.

4.3.2 Geogrid and compaction

When adding compaction to the layers of elements of the ballast and sub-ballast in contact with the geogrid, the rate at which the mechanical behaviour improves needs to be within the limits presented by the experimental study, which is of around 30% after 50000 cycles at 20Hz [6]. But, in this first phase, making use of the method used up until this point, the settlement is forecast based on a logarithmic function and, with that information, the change in mechanical properties is determined.

Due to the nature of the FEM, the ballast and sub-ballast were, as stated, modeled as a solid. This makes the direct accounting for Friction angle an impossibility, as there isn't a discrete element approach. So, in order to study how the change in mechanical properties of the volumes close to the geogrid change with the additional compactness and increased density, an experimental approach took place, with several FEM simulations being run.

Elastic properties

The first step was the analysis of the behaviour in the elastic domain, this was accomplished by gradually increasing the Young modulus (E) of the set of elements in contact with the geogrid from 10 to 50%. Each analysis was done by simulating, with the use of *ANSYS APDL*, the behaviour of the railway with FEM.

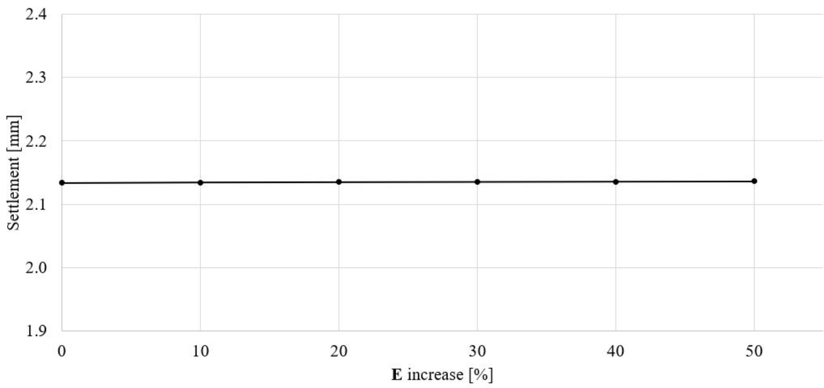

Figure 4.13: Change in settlement with the increase in Young modulus.

By increasing the Young modulus by 10% in each simulation, the change in behaviour was studied and, as presented in figure 4.13, the change in behaviour was negligible.

These results show that, in order to achieve the expected behaviour, a change in the plastic deformation mechanical parameters is crucial.

Plastic properties

With increased compactness, an increase in Young modulus is to be expected [40] and, even though the results presented in the previous sub-chapter (4.3.2) do not indicate a change in behaviour, a 10% increase is assumed.

The same interval of percentile increase was applied to both the tangent modulus and the yield tension, which is also from 10 to 50%.

A Design of Experiments was done, starting with a 2^4 factorial study of the evolution of settlement with the Yield tension and tangent modulus within 10 and 20%. In this first phase, the highest improvement was obtained with the following parameters (table 4.14):

Table 4.14: Percentile increase for each mechanical property in the second set of combinations.

	Sub-ballast	**Ballast**
Young modulus [%]	10	10
Yield tension [%]	20	20
Tangent modulus [%]	20	20

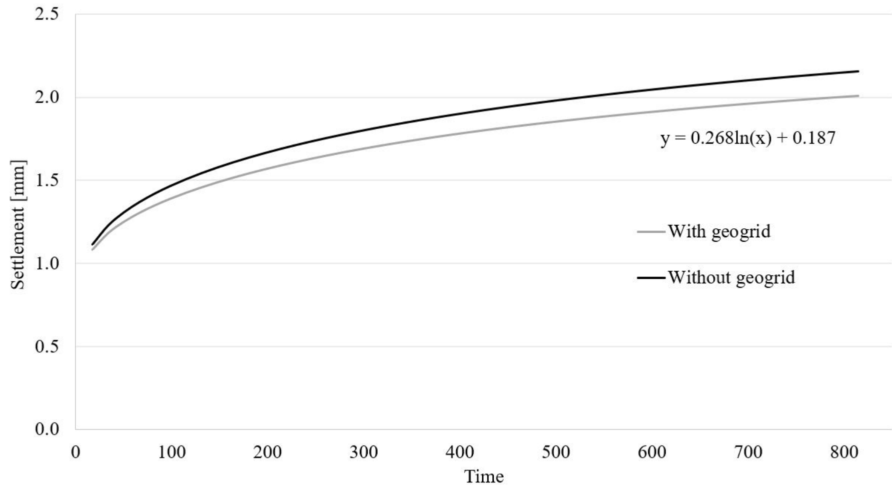

Figure 4.14: Railway behaviour with the changes presented in table 4.14.

The result of the settlement after compaction was 2.005 mm, which presents a 7.04% improvement and, although it is a significant improvement after just 50 cycles, by analysing the logarithmic function it is seen that it still doesn't reach the expected slope.

Since the slope, as shown in figure 4.3.2, being above the previously established, a new 2^4 factorial study was run, this time with the percentile increase being between 30 and 50%. With this approach, with the percentile increase presented in table 4.15, there is a better approximation of the behaviour of the railway, as shown by the logarithmic function in figure 4.15.

Table 4.15: Percentile increase for each mechanical property in the second set of combinations.

	Sub-ballast	**Ballast**
Young modulus [%]	10	10
Yield tension [%]	50	50
Tangent modulus [%]	50	50

With a final settlement of 1.905 mm, an improvement of 11.66% was presented, presenting no need further honing, as the results would be close to identical unless an even higher increase in mechanical properties was applied, which couldn't be done without further study into the behaviour of a railway, most notably ballast and sub-ballast and the elements further away from the geogrid.

The stress state ratio that exists within the structure (figure 4.16) is subject to changes when compared to what was shown previously in figure 4.16(a), as the stress spreads less over the ballast and sub-ballast due to the relevant role that the geogrid and compaction have in resisting the loads and resulting stress.

With the deformation being presented in figure 4.17 with a magnification of 170 times, the low distribution of vertical deformation when compared to figure 4.10 provides justification to the lower logarithmic slope behaviour of the settlement (figure 4.15) as,

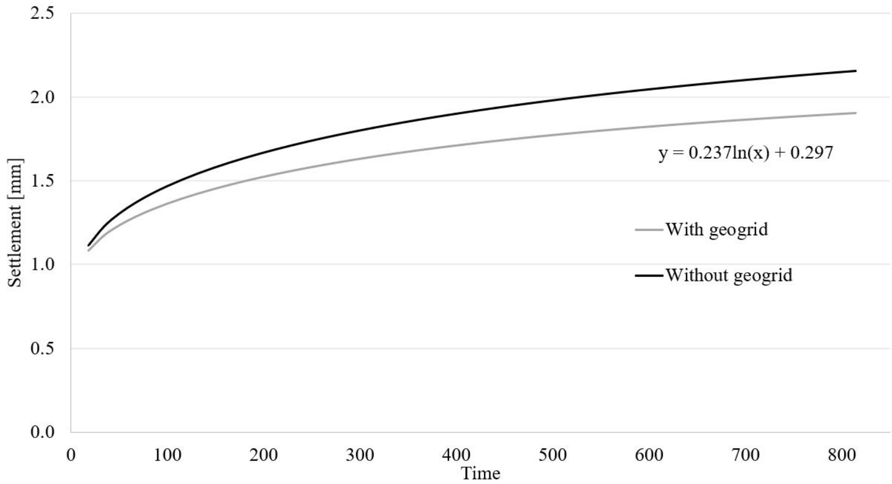

Figure 4.15: Railway behaviour with the modifications presented in table 4.15.

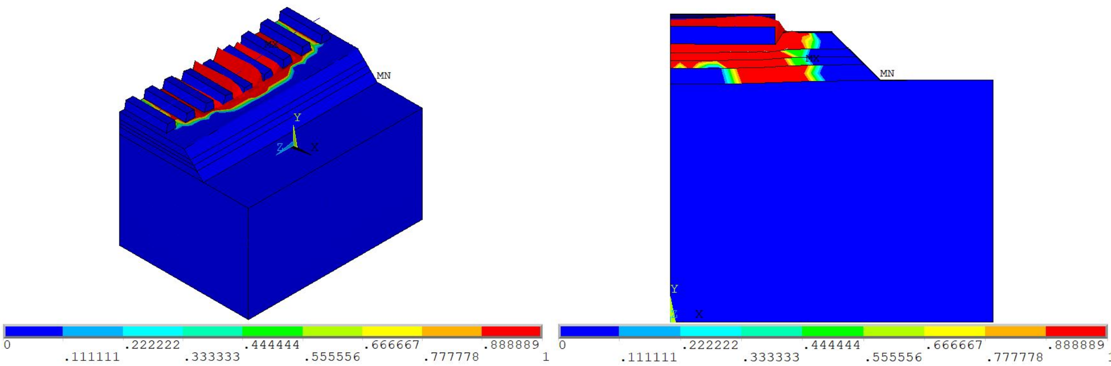

(a) Stress state ratio in isometric view

(b) Stress state ratio in section view

Figure 4.16: Stress state ratio within the model when under the influence of a geogrid.

when a smaller volume shows variation in shape, the overall deformation is lower along the cycles.

After the low impact felt by the settlement when the Young modulus is altered, the study of the effect caused by the modification of the yield tension and tangent modulus of the ballast and sub-ballast has relevancy when analysing how the compaction caused by the geogrid interacts with the structure. Thus, in table 4.16, the identification for each mechanical property is shown and, in figure 4.18, the effect for each property is presented.

Table 4.16: Appointment of letters to each property.

	Factor	Letter
Ballast	Yield tension	A
	Tangent modulus	B
Sub-ballast	Yield tension	C
	Tangent modulus	D

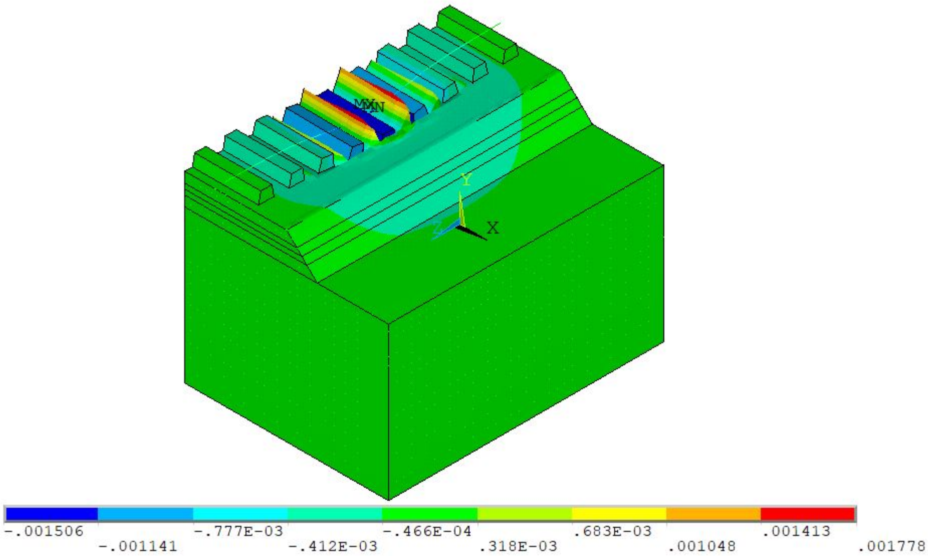

]Deformation of the model with the first application of load [m].

Figure 4.17: .

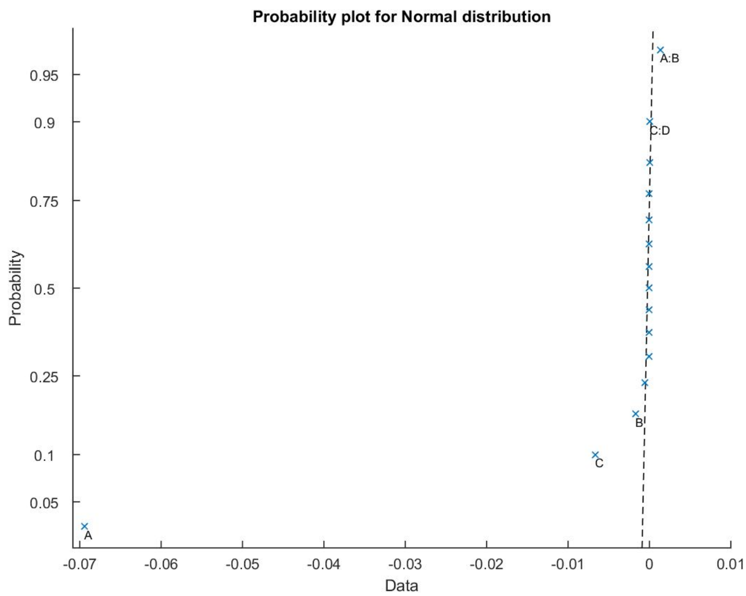

Figure 4.18: Effects for each plastic mechanical property n the settlement.

As presented in figure 4.18, the mechanical property which has the most impact in the change in behaviour is the yield tension, highlighting, as expected, the ballast. As demonstrated in the previous studies 2.4, the tangent modulus has a relatively low effect in the overall behaviour of the railway. According to the results presented, the increase in Friction angle results in higher yield tensions and tangent modulus while, despite it also being increased, the Young modulus doesn't have influence over the settlement. But, without further experimental studies, these results cannot be validated.

5

Conclusion and Future Work

The objective of this work was, as expressed, the development of a viable numerical model of a railway with the FEM, by making use of *ANSYS APDL* for the FEM and *Matlab* for the analytical study. The nature of the model makes it possible to analyse close to any track section.

Due to the limitations of the FEM, it isn't possible to account directly for the friction angle, so the chosen approach was the altering of the mechanical properties, which result of the change in Friction angle. Due to the way the compaction influences the structure, the behaviour of a railway with and without a geogrid is expected to be similar in the first few cycles, as the compaction which occurs in the layers closer to the geogrid tends to be gradual. But, since this similarity is seen mostly in the first few cycles, it is not accounted for in the modelling of this model.

With the mechanical changes that happen in the sections close to the railway, along with the improvement of the settlement, a geogrid proves to be an important addition to modern day railway transportation. Even though, with the improvements of 50% added to the mechanical properties of the elements close to the geoynthetic, the behaviour proved to be similar to what is seen in experimental studies. The change of those same properties might happen (in a lower scale) to the rest of the elements which compose the ballast and sub-ballast, especially when the mechanical properties have an improvement of over 50%.

Thus, due to the positive results obtained, the model proves to be a useful tool in the development of further research.

5.1 Future Work

With the dissertation being developed with the objective of being the basis for future research, there is still room for further development and some suggestions for such are:

- Development of a process of gradual compaction along the cycles;
- Study of short- and long-term (500000 cycles) behaviour;
- Study of the changes in behaviour when under dynamic conditions (transient analysis);
- Mitigate the discrepancy between the first peaks of the numerical and experimental models;
- Implement changes in the mechanical properties further away from the geogrid when compaction occurs.
- Impact analysis of the load under imperfect geometrical conditions of the railway.

Bibliography

[1] J. M. Lourenço. *The NOVAthesis LaTeX Template User's Manual*. NOVA University Lisbon. 2021. URL: https://github.com/joaomlourenco/novathesis/raw/master/template.pdf (cit. on p. ii).

[2] *Urgent action is needed to protect human health from the increasing effects of climate change | Elsevier Enhanced Reader*. URL: https://reader.elsevier.com/reader/sd/pii/S2542519619301147?token=B4B384B7AF839342124262887593CFB78C32EB4B03F09209055B6BBA10303284AB64810DB7F0C7762DE815B8238140DF&originRegion=eu-west-1&originCreation=20220209181824 (cit. on pp. 1, 5).

[3] I. Durazo-Cardenas et al. "An autonomous system for maintenance scheduling data-rich complex infrastructure: Fusing the railways' condition, planning and cost". In: *Transportation Research Part C: Emerging Technologies* 89 (2018-04), pp. 234–253. ISSN: 0968-090X. DOI: 10.1016/J.TRC.2018.02.010 (cit. on pp. 1, 7).

[4] M. Grygierek and J. Kawalec. "Selected Laboratory Research on Geogrid Impact on Stabilization of Unbound Aggregate Layer". In: *Procedia Engineering* 189 (2017-01), pp. 484–491. ISSN: 1877-7058. DOI: 10.1016/J.PROENG.2017.05.078 (cit. on p. 2).

[5] *Geogrids – GEOMAT*. URL: https://www.geomat.eu/en/geogrids (cit. on pp. 3, 4).

[6] S. K. K. Hussaini and K. Sweta. "Application of Geogrids in Stabilizing Rail Track Substructure". In: *Frontiers in Built Environment* 6 (2020-02). ISSN: 22973362. DOI: 10.3389/FBUIL.2020.00020/FULL (cit. on pp. 5, 7, 24, 25, 41, 49, 50).

[7] M. Esmaeili, S. Farsi, and A. Shamohammadi. "Effect of rock strength on the degradation of ballast equipped with under sleeper pad". In: *Construction and Building Materials* 321 (2022-02), p. 126413. ISSN: 0950-0618. DOI: 10.1016/J.CONBUILDMAT.2022.126413 (cit. on pp. 5, 6).

[8] P. A. Costa, R. Calçada, and A. S. Cardoso. "Ballast mats for the reduction of railway traffic vibrations. Numerical study". In: *Soil Dynamics and Earthquake Engineering* 42 (2012-11), pp. 137–150. ISSN: 0267-7261. DOI: 10.1016/J.SOILDYN.2012.06.014 (cit. on pp. 5, 7).

[9] *Application of Ocean Geogrids in Railways* -. URL: https://oceangeosynthetics.com/application-of-ocean-geogrids-in-railways/ (cit. on p. 5).

[10] *Track Geotechnology and Substructure Management - Ernest Theodore Selig, John M. Waters - Google Livros*. URL: https://books.google.pt/books?hl=pt-PT&lr=&id=ZHxW4D6XT0MC&oi=fnd&pg=PA10&dq=Track+Geotechnology+and+Substructure+Management&ots=jpYADUqKgS&sig=kXj6u7LWdSf4nPCky5zOkwLFwsk&redir_esc=y#v=onepage&q=Track%5C%20Geotechnology%5C%20and%5C%20Substructure%5C%20Management&f=false (cit. on p. 5).

[11] M. Sol-Sánchez and G. D'Angelo. "Review of the design and maintenance technologies used to decelerate the deterioration of ballasted railway tracks". In: *Construction and Building Materials* 157 (2017-12), pp. 402–415. ISSN: 0950-0618. DOI: 10.1016/J.CONBUILDMAT.2017.09.007 (cit. on pp. 6, 7).

[12] J. I. Egana, J. Vinolas, and M. Seco. "Investigation of the influence of rail pad stiffness on rail corrugation on a transit system". In: *Wear* 261 (2 2006-07), pp. 216–224. ISSN: 0043-1648. DOI: 10.1016/J.WEAR.2005.10.004 (cit. on p. 6).

[13] S. Kaewunruen and A. Remennikov. "An Experimental Evaluation of the Attenuation Effect of Rail Pad on Flexural An Experimental Evaluation of the Attenuation Effect of Rail Pad on Flexural Behaviour of Railway Concrete Sleeper under Severe Impact Loads Behaviour of Railway Concrete Sleeper under Severe Impact Loads". In: (2008). URL: https://ro.uow.edu.au/engpapershttps://ro.uow.edu.au/engpapers/469https://ro.uow.edu.au/engpapers/469 (cit. on p. 6).

[14] A. Johansson et al. "Under sleeper pads—Influence on dynamic train–track interaction". In: *Wear* 265 (9-10 2008-10), pp. 1479–1487. ISSN: 0043-1648. DOI: 10.1016/J.WEAR.2008.02.032 (cit. on p. 6).

[15] T. N. Ngo, B. Indraratna, and C. Rujikiatkamjorn. "Improved performance of ballasted tracks under impact loading by recycled rubber mats". In: *Transportation Geotechnics* 20 (2019-09), p. 100239. ISSN: 2214-3912. DOI: 10.1016/J.TRGEO.2019.04.002 (cit. on p. 7).

[16] L. Horníček et al. "An investigation of the effect of under-ballast reinforcing geogrids in laboratory and operating conditions". In: *Proceedings of the Institution of Mechanical Engineers, Part F: Journal of Rail and Rapid Transit* 224 (4 2010-01), pp. 269–277. ISSN: 09544097. DOI: 10.1243/09544097JRRT330 (cit. on pp. 7, 24, 25, 30, 34, 35, 41, 47, 62).

[17] J. G. Rose and M. J. Hensley. "Performance of Hot-Mix-Asphalt Railway Trackbeds". In: () (cit. on p. 7).

[18] B. M. Das and D. Emeritus. "Use of Geogrid in Subgrade-Ballast System of Railroads Subjected to Cyclic Loading for Reducing Maintenance". In: () (cit. on p. 7).

[19] A. Miri et al. “Mitigation of track buckling in transition zones of steel bridges by geotextile reinforcement of the ballast layer”. In: *Geotextiles and Geomembranes* 50 (2022), pp. 282–292. DOI: 10.1016/j.geotexmem.2021.11.006. URL: https://doi.org/10.1016/j.geotexmem.2021.11.006 (cit. on p. 7).

[20] A. L. de Melo et al. “Methods to Monitor and Evaluate the Deterioration of Track and Its Components in a Railway In-Service: A Systemic Review”. In: *Frontiers in Built Environment* 6 (2020-09), p. 118. ISSN: 22973362. DOI: 10.3389/FBUIL.2020.00118/BIBTEX (cit. on p. 8).

[21] C. Vale and I. M. Ribeiro. *Railway condition-based maintenance model with stochastic deterioration*. 2014. URL: https://journals.vilniustech.lt/index.php/JCEM/article/view/3163/2625 (cit. on p. 8).

[22] M. El-Sibaie and Y.-J. Zhang. “Objective Track Quality Indices”. In: *Transportation Research Record* 1863.1 (2004), pp. 81–87. DOI: 10.3141/1863-11. eprint: https://doi.org/10.3141/1863-11. URL: https://doi.org/10.3141/1863-11 (cit. on p. 8).

[23] *Plasser American - Machines Systems - Track recording and measuring*. URL: https://www.plasseramerican.com/en/machines-systems/measuring-work-em-120.html (cit. on p. 8).

[24] S. Fontul et al. “Railways Track Characterization Using Ground Penetrating Radar”. In: *Procedia Engineering* 143 (2016-01), pp. 1193–1200. ISSN: 1877-7058. DOI: 10.1016/J.PROENG.2016.06.120 (cit. on p. 8).

[25] H. Wang et al. “Study of loaded versus unloaded measurements in railway track inspection”. In: *Measurement: Journal of the International Measurement Confederation* 169 (2021-02). ISSN: 02632241. DOI: 10.1016/J.MEASUREMENT.2020.108556 (cit. on p. 9).

[26] C. A. Murray, W. A. Take, and N. A. Hoult. “Measurement of vertical and longitudinal rail displacements using digital image correlation”. In: *Canadian Geotechnical Journal* 52 (2 2015), pp. 141–155. ISSN: 12086010. DOI: 10.1139/CGJ-2013-0403/ASSET/IMAGES/CGJ-2013-0403TAB3.GIF. URL: https://cdnsciencepub.com/doi/abs/10.1139/cgj-2013-0403 (cit. on p. 9).

[27] T. Karis. *Correlation between Track Irregularities and Vehicle Dynamic Response Based on Measurements and Simulations*. ISBN: 9789177297765 (cit. on p. 10).

[28] C. Esveld. “Modern Railway Track Second Edition”. In: () (cit. on p. 10).

[29] J. A. Schey. “Introduction to manufacturing processes”. In: (2000), p. 962 (cit. on p. 12).

[30] A. P. Boresi and R. J. Schmidt. *Advanced Mechanics of Materials*. 6th edition. Hoboken, NJ: Wiley, 2002. ISBN: 9780471438816 (cit. on p. 12).

[31] A. Inc. *4.2. Rate-Independent Plasticity*. URL: https://www.mm.bme.hu/~gyebro/files/ans_help_v182/ans_thry/thy_mat1.html (cit. on p. 13).

[32] R. Hurlston. *Isotropic, Kinematic Or Mixed-Mode? Which Hardening Model For Your Abaqus FEA Analysis?* 2021-01. URL: https://www.fidelisfea.com/post/isotropic-kinematic-or-mixed-mode-which-hardening-model-for-your-abaqus-fea-analysis (cit. on p. 13).

[33] F. F. dos Santos. "Railway Track Numerical Modelling with Geogrid Incorporation". MSc Theses. Nova School of Science and Technology, 2021-11, pp. 21–47 (cit. on pp. 14, 27, 28, 30).

[34] A. Inc. *BEAM188*. 2018. URL: https://www.mm.bme.hu/~gyebro/files/ans_help_v182/ans_elem/Hlp_E_BEAM188.html (cit. on pp. 14, 31).

[35] A. Inc. *SOLID185*. 2018. URL: https://www.mm.bme.hu/~gyebro/files/ans_help_v182/ans_elem/Hlp_E_SOLID185.html (cit. on pp. 15, 30, 31).

[36] A. Inc. *COMBIN14*. 2018. URL: https://www.mm.bme.hu/~gyebro/files/ans_help_v182/ans_elem/Hlp_E_COMBIN14.html (cit. on pp. 16, 31).

[37] A. Inc. *SHELL181*. 2018. URL: https://www.mm.bme.hu/~gyebro/files/ans_help_v182/ans_elem/Hlp_E_SHELL181.html (cit. on pp. 16, 30).

[38] D. C. Montgomery. *Design and analysis of experiments*. 3rd. John Wiley Sons, 1991 (cit. on pp. 17–21, 23, 24).

[39] A. F. da Silva Rodrigues. "Viability and Applicability of Simplified Models for the Dynamic Analysis of Ballasted Railway Tracks". PHD Thesis. Faculdade de Ciências e Tecnologia, Universidade Nova de Lisboa, 2017-06. URL: http://hdl.handle.net/10362/21663 (cit. on pp. 25, 27, 28, 31, 33, 35, 46).

[40] P. Breul and G. Saussine. "On site mechanical characterization of the ballast state". In: *Periodica Polytechnica Civil Engineering* 55 (1 2011), pp. 31–38. ISSN: 15873773. DOI: 10.3311/pp.ci.2011-1.04 (cit. on pp. 26, 51).

[41] ArcelorMittal. *Transport Rails European Standards*. 2021. URL: https://rails.arcelormittal.com/types-rails/transport-rails/european-standards (cit. on p. 32).

[42] S. S. Rao. *Mechanical Vibrations In Si Units*. Ed. by J. H. Horton, N. Dias, and M. Bayman. 6th. Pearson Education Limited, 2018, pp. 153–403 (cit. on pp. 32, 33).

A

Results of the Monte Carlo method

In this table, the results for each test is presented along with the sum and euclidean norm of the errors of each test against the experimental results [16].

	Effects						Error	
	A	B	C	D	E	F	**Sum**	**Norm**
Test 1								
All effects	1.465	1.342	-1.487	1.443	-1.486	0.310	22.978	13.036
Significant effects	1.465	1.342	-1.487	1.443	-1.486	0.310	23.597	13.689
Test 2								
All effects	1.466	1.343	-1.405	1.497	-1.421	0.685	22.071	13.540
Significant effects	1.466	1.343	-1.405	1.497	-1.421	0.685	23.164	13.909
Test 3								
All effects	1.382	1.396	-1.078	1.238	-1.451	0.043	26.795	14.544
Significant effects	1.382	1.396	-1.078	1.238	-1.451	0.043	28.515	15.294
Test 4								
All effects	1.382	1.315	-1.441	1.409	-1.223	0.482	23.952	14.439
Significant effects	1.382	1.315	-1.441	1.409	-1.223	0.482	24.984	14.868
Test 5								
All effects	1.489	1.472	-1.207	0.038	-1.318	1.249	27.979	20.635
Significant effects	1.489	1.472	-1.207	0.038	-1.318	1.249	28.964	21.011
Test 6								
All effects	1.476	1.229	-1.174	1.058	-1.324	1.055	25.825	16.949
Significant effects	1.476	1.229	-1.174	1.058	-1.324	1.055	26.133	17.075
Test 7								
All effects	1.479	1.287	-1.207	0.372	-1.149	0.739	27.218	17.004
Significant effects	1.479	1.287	-1.207	0.372	-1.149	0.739	27.132	16.940
Test 8								
All effects	1.477	1.235	-1.297	1.469	-0.822	0.594	27.812	17.001
Significant effects	1.477	1.235	-1.297	1.469	-0.822	0.594	27.576	17.140

Test 9								
All effects	0.961	1.417	-1.352	0.856	-1.389	0.067	29.697	15.927
Significant effects	0.961	1.417	-1.352	0.856	-1.389	0.067	30.967	16.542
Test 10								
All effects	0.974	1.410	-1.477	1.076	-1.435	0.758	26.723	15.704
Significant effects	0.974	1.410	-1.477	1.076	-1.435	0.758	27.226	15.887
Test 11								
All effects	0.875	1.371	-1.398	1.486	-1.455	0.184	26.529	14.759
Significant effects	0.875	1.371	-1.398	1.486	-1.455	0.184	28.313	15.470
Test 12								
All effects	0.874	1.327	-1.483	1.270	-1.382	0.362	26.176	15.307
Significant effects	0.874	1.327	-1.483	1.270	-1.382	0.362	27.492	15.797
Test 13								
All effects	0.958	1.282	-1.489	-0.129	-1.458	1.435	25.579	18.102
Significant effects	0.958	1.282	-1.489	-0.129	-1.458	1.435	26.817	18.637
Test 14								
All effects	0.753	1.348	-1.344	1.057	-1.253	0.708	28.978	17.106
Significant effects	0.753	1.348	-1.344	1.057	-1.253	0.708	29.433	17.216
Test 15								
All effects	0.867	1.229	-0.806	1.422	-1.286	0.534	30.751	18.256
Significant effects	0.867	1.229	-0.806	1.422	-1.286	0.534	30.595	18.490
Test 16								
All effects	0.974	1.410	-1.477	1.076	-1.435	0.758	26.723	15.704
Significant effects	0.974	1.410	-1.477	1.076	-1.435	0.758	27.226	15.887

2023 Development and improvement of a numerical model to simulate the mechanical behaviour of railways Marcelo Menezes

NOVA SCHOOL OF SCIENCE & TECHNOLOGY